Eur. J. Mineral.
2017, **29**, 101–116
Published online 3 February 2017

Khesinite, $Ca_4Mg_2Fe^{3+}_{10}O_4[(Fe^{3+}_{10}Si_2)O_{36}]$, a new rhönite-group (sapphirine supergroup) mineral from the Negev Desert, Israel – natural analogue of the SFCA phase

IRINA O. GALUSKINA[1,*], EVGENY V. GALUSKIN[1], ANNA S. PAKHOMOVA[2], REMO WIDMER[3], THOMAS ARMBRUSTER[3], BILJANA KRÜGER[4], EDWARD S. GREW[5], YEVGENY VAPNIK[6], PIOTR DZIERAŻANOWSKI[7] and MIKHAIL MURASHKO[8]

[1] Faculty of Earth Sciences, Department of Geochemistry, Mineralogy and Petrography, University of Silesia, Będzińska 60, 41-200 Sosnowiec, Poland
*Corresponding author, e-mail: irina.galuskina@us.edu.pl
[2] University of Bayreuth, Bayerisches Geoinstitut, Universitätsstraße 30, 95447 Bayreuth, Germany
[3] Mineralogical Crystallography, Institute of Geological Sciences, University of Bern, Baltzerstr. 1–3, 3012 Bern, Switzerland
[4] Institute of Mineralogy Petrography, University of Innsbruck, Innrain 52, 6020 Innsbruck, Austria
[5] School of Earth and Climate Sciences, University of Maine, Orono, ME 04469-5790, USA
[6] Department of Geological and Environmental Sciences, Ben-Gurion University of the Negev, P.O.B. 653, Beer-Sheva 84105, Israel
[7] Institute of Geochemistry, Mineralogy and Petrology, Warsaw University, Al. Zwirki i Wigury 93, 02-089 Warszawa, Poland
[8] Saint Petersburg State University, Faculty of Geology, Universitetskaya nab. 7-9, St. Petersburg 199034, Russia

Abstract: Khesinite, $Ca_4Mg_2Fe^{3+}_{10}O_4(Fe^{3+}_{10}Si_2)O_{36}$, is a new member of the rhönite group of the sapphirine supergroup. Khesinite was discovered in thin veins of paralavas within fine-grained gehlenite rocks (hornfels) of the Hatrurim Complex in the Negev Desert, Israel. Paralavas are composed of rankinite, pseudowollastonite (rarely wollastonite), flamite, kalsilite, cuspidine and members of the solid-solution series: schorlomite–andradite, gehlenite–ackermanite–"Fe^{3+}-gehlenite", magnesioferrite–spinel and fluorapatite–fluorellestadite. Accessory and rare minerals are represented by baryte, walstromite, fresnoite, vorlanite, barioferrite, hematite, perovskite, gurimite, zadovite, aradite and hexacelsian. Electron-microprobe analysis of the holotype khesinite gives the following empirical formula for 40 oxygens and 28 cations: $Ca_4(Fe^{3+}_{8.528}Mg_{1.635}Ca_{0.898}Ti^{4+}_{0.336}Ni^{2+}_{0.217}Mn^{2+}_{0.155}Cr^{3+}_{0.132}Fe^{2+}_{0.098})_{\Sigma 12}[(Fe^{3+}_{6.827}Al_{2.506}Si_{2.667})_{\Sigma 12}O_{40}]$. Khesinite is black to dark brown. It has semi-metallic lustre and does not show fluorescence. Cleavage and parting are not observed, fracture is irregular. Khesinite has a Mohs' hardness of 6; microhardness VHN_{50} is 943 kg mm^{-2}. The calculated density is 4.097 g cm^{-3}. In reflected light khesinite is grey with weak internal brown reflections. Reflectance data for the COM (Commission of Ore Mineralogy, IMA) wavelengths vary from ~13.4% (470 nm) to ~11.8% (700 nm). The crystal structure of khesinite [$P\overline{1}$ $a = 10.5363(1)$, $b = 10.9242(2)$, $c = 9.0612(1)$ Å, $\alpha = 106.340(1)°$, $\beta = 95.765(1)°$, $\gamma = 124.373(1)°$, $V = 780.54(2)$ Å^3] was refined from X-ray single-crystal data to $R_1 = 0.046$. The khesinite structure is close to that of the synthetic compounds SFCA and SFCAM. Khesinite crystallized in paralava from melt, sometimes forming isolated crystals, but more commonly reaction rims on magnesioferrite in association with pseudowollastonite and flamite at temperature not lower than 1200 °C.

Key-words: khesinite; new mineral; rhönite group; sapphirine supergroup; crystal structure; Raman; dorrite; ferrites; SFCA; SFCAM; pyrometamorphism; Hatrurim Complex.

1. Introduction

Khesinite (IMA2014-033), $Ca_4Mg_2Fe^{3+}_{10}O_4(Fe^{3+}_{10}Si_2)O_{36}$ [$P\overline{1}$, $a = 10.5363(1)$, $b = 10.9242(2)$, $c = 9.0612(1)$ Å, $\alpha = 106.340(1)°$, $\beta = 95.765(1)°$, $\gamma = 124.373(1)°$, $V = 780.54(2)$ Å^3], the tetrahedral Fe^{3+}-dominant analogue of dorrite, $Ca_4(Mg_3Fe^{3+}_9)O_4(Si_3Al_8Fe^{3+})O_{36}$ [$a = 10.505(3)$, $b = 10.897(3)$, $c = 9.019(1)$ Å, $\alpha = 106.26(2)°$, $\beta = 95.16(2)°$, $\gamma = 124.75(2)°$; $V = 772.5(4)$ Å^3; Cosca *et al.*, 1988; Grew *et al.*, 2008], was discovered in thin veins of paralava in fine-grained gehlenite rocks (hornfels) of the Hatrurim Complex outcropping in the Negev Desert close to the city of Arad, Israel. The Hatrurim Basin is an area where rocks of the Hatrurim Complex ("Mottled Zone") containing larnite, gehlenite and spurrite are exposed; it is the largest such exposure in Israel (Bentor, 1960; Gross, 1977; Vapnik *et al.*, 2007; Novikov *et al.*, 2013).

DOI: 10.1127/ejm/2017/0029-2589
0935-1221/17/0029-2589 $ 7.20

Khesinite was originally approved by CNMNC-IMA with a formula $Ca_4(Mg_3Fe^{3+}{}_9)O_4[Fe^{3+}{}_9Si_3O_{36}]$ by analogy with dorrite (Grew *et al.*, 2008). However, this formula is not a proper end-member and, in our opinion, should be changed to $Ca_4Mg_2Fe^{3+}{}_{10}O_4[(Fe^{3+}{}_{10}Si_2)O_{36}]$ to comply with CNMNC-IMA recommendations. By extension, the dorrite formula should also be changed to $Ca_4Mg_2Fe^{3+}{}_{10}O_4[(Al_{10}Si_2)O_{36}]$ (see the Discussion section).

The name khesinite is given in honour of the well-known USSR and Israeli geophysicist Boris Emmanuilovich Khesin (1932–2010). He was a leading geophysicist in Azerbaijan. Prof. B.E. Khesin was the author of more than 260 scientific works including 10 monographs. In 1991, he began to work at the Department of Geological and Environmental Sciences of the Ben-Gurion University of the Negev, Beer-Sheva, Israel. During the last years of his life, he was engaged in a geophysical study of the Hatrurim Complex. Several of his last papers consider the genesis of the Hatrurim Complex and its significance for the prospecting of hydrocarbon deposits in the Levant.

Type material is deposited in the collections of the Museum of Natural History in Bern, Bernastrasse 5, 3005 Bern, Switzerland, catalogue number NMBE 4717.

In the present paper, we give data on the composition and structure of the new mineral khesinite in the holotype specimen from the Negev Desert, Israel and analytical data on khesinite from specimens collected in paralava and gehlenite hornfels of the Hatrurim Complex from other localities in the Judean Mountains and Negev Desert. We discuss aspects of its genesis and formal criteria for defining a proper end-member formula.

2. Background

Minerals of the dorrite–khesinite series, including a single composition corresponding to high-Al khesinite, were described in paralavas of the Powder River Basin, Wyoming (Cosca et al., 1988) as well as in buchite at Buffalo, Wyoming [Fe^{3+}-rich "melilite" of Foit *et al.* (1987)]. The first report of a mineral close to khesinite in composition in the Hatrurim Complex concerned a few grains in gehlenite hornfels at the Nabi Musa locality, Judean Desert (Sokol *et al.*, 2011).

Khesinite is close in composition to the anthropogenic phase "malakhovite" from the burned dumps of the Chelyabinsk coal basin, Urals, Russia (Chesnokov *et al.*, 1993). Ferrite from pyrometamorphic oil-shale slags in Lapanouse, Sévérac-le-Château, Aveyron, France, for which Gatel *et al.* (2015) erroneously gave the formula $CaFe_4O_7$, is an anthropogenic analogue of khesinite. Záček *et al.* (2015) reported a calcium ferrite from esseneite–melilite paralava at Zelénky, Czech Republic as $CaFe_4O_7$, but this formula is not correct for this ferrite because the presence of significant Si, Al and Mg was overlooked. Holotype khesinite is close to the synthetic compounds SFCA and SFCAM (Mumme, 1988; Hamilton *et al.*, 1989; Sugiyama *et al.*, 2005; Liles *et al.*, 2016).

Khesinite is a new member of the rhönite group, one of the groups constituting the sapphirine supergroup (Grew *et al.*, 2008; Mills *et al.*, 2009). A general formula of minerals of the rhönite group can be written as $Ca_4M_{12}O_4[T_{12}O_{36}]$ or, more simply, $Ca_4M_{12}T_{12}O_{40}$, where M represents the seven octahedral sites, which are occupied by Fe^{3+}, Fe^{2+}, Mg, Al, Sc, Ti^{4+}, V^{3+}, Cr^{3+}, Ca and Sb^{5+}, and T represents the six tetrahedral sites, which are occupied by Fe^{3+}, Al, Si, Be and B. One of the M sites, $M7$, is considered separately from the other M sites in distinguishing some species. Khesinite, $Ca_4Mg_2Fe^{3+}{}_{10}O_4(Fe^{3+}{}_{10}Si_2)O_{36}$, differs from other minerals of this group in that Fe^{3+} is dominant at both M and T sites. As the formulation of the rhönite group by Grew *et al.* (2008), several new minerals have been added to this group: kuratite (IMA2013-109) $Ca_4(Fe^{2+}{}_{10}Ti_2)O_4[Si_8Al_4O_{36}]$ (Hwang *et al.*, 2014), warkite $Ca_4Sc_{12}O_4[Al_{12}O_{36}]$ (IMA2013-129) (Ma *et al.*, 2014), beckettite (IMA2015-001) $Ca_4V_{12}O_4[Al_{12}O_{36}]$ (Ma *et al.*, 2015) and addibischoffite (IMA2015-006) $Ca_4Al_{12}O_4[Al_{12}O_{36}]$ (Ma & Krot, 2015).

3. Methods of investigations

The crystal morphology and chemical composition of khesinite and associated minerals were studied using optical microscopes, analytical scanning electron microscopes (Philips XL30 ESEM/EDAX and Phenom XL, Faculty of Earth Sciences, University of Silesia) and electron microprobe analyzer CAMECA SX100 (Institute of Geochemistry, Mineralogy and Petrology, University of Warsaw). Electron-probe microanalyses of khesinite and associated minerals were performed at 15 kV, 20 nA and 1–3 μm beam diameter using the following lines and standards: Ca$K\alpha$, Si$K\alpha$ = wollastonite; Al$K\alpha$, K$K\alpha$ = orthoclase; Cr$K\alpha$ = Cr_2O_3; Fe$K\alpha$ = hematite; Mn$K\alpha$ = rhodochrosite; Ti$K\alpha$ = rutile; Mg$K\alpha$ = diopside; Na$K\alpha$ = albite; Ba$L\alpha$, S$K\alpha$ = baryte; P$K\alpha$ = apatite; Sr$L\alpha$ = $SrTiO_3$, Cu$K\alpha$ = Cu_2O; Ni$K\alpha$ = NiO; Zr$L\alpha$ = zircon, Zn$K\alpha$ = sphalerite; V$K\alpha$ = V_2O_5.

A single-crystal X-ray study of khesinite was carried out using a Bruker APEX II SMART diffractometer (Mo$K\alpha$ radiation, $\lambda = 0.71073$ Å, University of Bern, Switzerland). Data were processed using SAINT (Bruker, 2012). An empirical absorption correction using SADABS (Sheldrick, 1996) was applied. The structure was solved by direct methods, with subsequent analyses of difference-Fourier maps, and refined with neutral-atom scattering factors using SHELXL (Sheldrick, 2008).

The Raman spectrum of khesinite was recorded on a WITec confocal CRM alpha 300 Raman microscope (Faculty of Earth Sciences, University of Silesia) equipped with an air-cooled solid-state laser (532 nm) and a CCD camera operating at −61 °C. The laser radiation was coupled to a microscope through a single-mode optical fibre with a diameter of 3.5 μm. An air Olympus EPIPLAN 100/0.75 objective was used. The Raman scattered light was focused on a multi-mode fibre (30-μm diameter) and monochroma-

tor with a 600-mm^{-1} grating. The power of the laser on the sample was 10–20 mW. Some 20–30 scans with integration time of 3–5 s and a resolution of 3 cm^{-1} were collected and averaged. The monochromator was calibrated using the Raman scattering line of a silicon plate (520.7 cm^{-1}). The fitting of the molecular spectra was realized by means of GRAMS/AI Version 9 Spectroscopy Software using a mixed Lorentzian + Gaussian function.

4. Occurrence and physicochemical properties

Homogeneous crystals of dark khesinite were detected in specimen no. IS-58, which consists of a brown, fine-grained gehlenite hornfels and coarse-grained paralava with visible dark schorlomite and long-prismatic greenish fluorapatite–fluorellestadite crystals (Figs. 1 and 2a). The specimen was collected at the Gurim anticline (the Hatrurim Basin) located near Arad city in the Negev Desert, Israel (31°09′N 35°17′E). Khesinite grains generally do not exceed 200 μm in size and are characterized by an irregular outline, although a few crystal faces are usually present. Rarely, khesinite grains attain a length of 400 μm or cluster in aggregates (Figs. 1c–e and 2a). It is necessary to note that we use the term "paralava" conditionally as these rocks are represented by coarse-grained rankinite–schorlomite–pseudowollastonite veins resembling pegmatites ("parapegmatite") with characteristic eutectic structures of, *e.g.*, schorlomite + flamite, gehlenite + flamite, kalsilite + flamite (Gfeller *et al.*, 2015; Sokol *et al.*, 2015).

These paralavas are composed of relatively large rankinite and pseudowollastonite (rarely wollastonite) crystals, which in places attain 2–3 cm in size, and also by minerals represented by solid solutions: schorlomite–andradite–grossular, gehlenite-ackermanite-"Fe^{3+}-gehlenite", magnesioferrite–spinel–trevorite–magnetite–cuprospinel–hercynite, fluorapatite–fluorellestadite (Fig. 1a). Less frequently large aggregates of kalsilite and cuspidine are noted. Accessory and rare minerals are represented by baryte, walstromite, fresnoite, vorlanite, barioferrite, hematite and perovskite (Figs. 1c and 2a) and also the recently discovered new Ba-bearing minerals: gurimite, zadovite, aradite and hexacelsian (Galuskina *et al.*, 2013, 2015; Galuskin *et al.*, 2015). In paralava, there are many small vesicles, which are filled by secondary, low-temperature minerals such as ettringite, calcite, apophyllite, afwillite, tobermorite and other unidentified Ca-hydrosilicates, commonly Cl-bearing.

Khesinite is black and translucent with a dark-brown colour in very thin edges (Fig. 1e). It has a semi-metallic lustre and does not show fluorescence. Cleavage and parting are not observed; fracture is irregular. Khesinite has a Mohs' hardness of 6, measured by Vickers hardness test with 50 g load. The resulting indentation corresponds to Vickers hardness 859–1001 with a mean (of 12) of 943 (44) kg mm^{-2}. Density could not be measured because of the small grain size. The calculated density is 4.097 g cm^{-3} using the empirical formula.

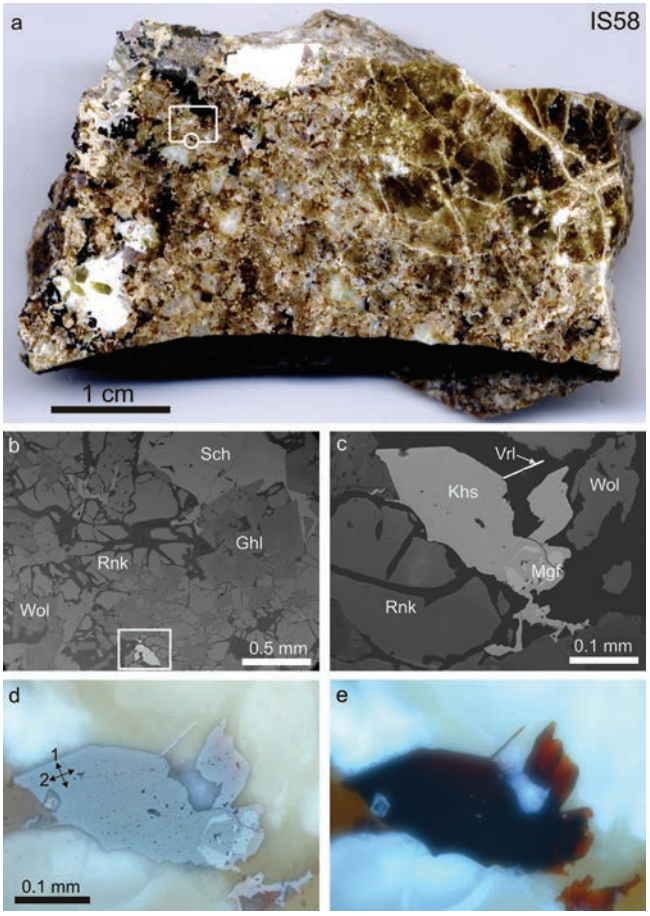

Fig. 1. (a) Holotype specimen no. IS-58 of paralava with conspicuous dark-brown schorlomite crystals. Fragment magnified in (b) is shown in a frame; fragment magnified in (c–e) is shown in a circle; (b) rankinite–schorlomite–pseudowollastonite–gehlenite paralava with khesinite crystal, fragment magnified in (c–e) is shown in a frame, backscattered-electron (BSE) image; (c–e) khesinite crystal with magnesioferrite relics: (c) – BSE image; (d and e) – reflected light: (d) – plane-polarized light, orientations of crystals at reflectivity measurements are shown by double-ended arrows (see Fig. S1 in Supplementary Material); (e) – cross-polarized light. Ghl – gehlenite, Khs – khesinite, Mgf – magnesioferrite, Rnk – rankinite, Sch – schorlomite, Wol – pseudowollastonite, Vrl – vorlanite.

In reflected light, khesinite shows grey colour (Fig. 1d) and weak brown internal reflections; pleochroism is very weak, birefringence and anisotropy are weak. Reflectance values measured in air using Zeiss SiC reflectance standard 182, number 472 (λ [nm], R_{max}/R_{min}) are as follows: 470, 14.05/12.73; 546, 13.17/12.08; 589, 12.78/11.76; 650, 12.48/11.55; 700, 12.32/11.42 (Fig. S1 and Table S1 in Supplementary Material, linked to this article and freely available from the GSW website of the journal, http://eurjmin.geoscienceworld.org/).

The composition of holotype khesinite (Table 1, analysis 1; sample IS-58) corresponds to the empirical formula: $Ca_4(Fe^{3+}_{8.528}Mg_{1.635}Ca_{0.898}Ti^{4+}_{0.336}Ni^{2+}_{0.217}Mn^{2+}_{0.155}Cr^{3+}_{0.132}Fe^{2+}_{0.098})_{\Sigma 12}[(Fe^{3+}_{6.827}Al_{2.506}Si_{2.667})_{\Sigma 12}O_{40}]$, which can be simplified to $\sim Ca_4(Fe^{3+}{}_9Mg_2Ca)_{\Sigma 12}(Fe^{3+}{}_7Al_2Si_3)_{\Sigma 12}O_{40}$.

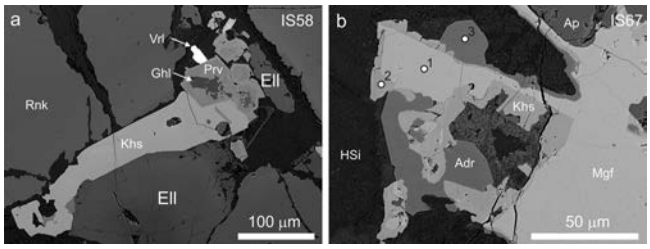

Fig. 2. (a) Khesinite grains used for Raman study and microhardness measurements (specimen no. IS58, points of Raman measurements are marked by A and B, see Fig. 3). Association of khesinite with Si–Fe^{3+}-bearing perovskite and vorlanite $CaUO_4$, BSE image; (b) overgrowths of khesinite and andradite on magnesioferrite (specimen no. IS67). Points of analyses given in Table 6 correspond to the numbers shown in (b), BSE image. Khs – khesinite, Rnk – rankinite, Ghl – melilite, Vrl – vorlanite, Prv – perovskite, Ell – fluorellestadite–fluorapatite, HSi – unidentified Ca-hydrosilicates, Ap – fluorapatite, Mgf – magnesioferrite, Adr – andradite.

The following main bands in the Raman spectrum (cm^{-1}, Fig. 3) are: overtones – 1638, 1495, 1403, 1132; TO$_4$ stretching – 947 $(SiO_4)^{4-}$, 814 and 749$(AlO_4)^{5-}$, 696 $(Fe^{3+}O_4)^{5-}$; MO$_6$ stretching, T–O–T stretching and bending modes, TO$_4$ bending modes – 610, 522, 481; MO$_6$ bending, TO$_4$ bending and TO$_4$ rotation modes – 310, 256; Ca-related vibrations – 159, 121. The interpretation of the Raman spectra of khesinite is complicated by superposition of bands from MO$_6$ stretching, T–O–T stretching and bending modes, TO$_4$ bending modes for different types of tetrahedra and octahedra. Nevertheless, bands from Fe^{3+}–O stretching vibrations at tetrahedral sites ~700 cm^{-1} $\nu_1(Fe^{3+}O_4)^{5-}$ and octahedral sites – 610 cm^{-1} $\nu_1(Fe^{3+}O_6)^{9-}$ and also bending vibrations $\nu_2(Fe^{3+}O_4)^{5-}$ near 310 cm^{-1} are characteristic for khesinite. Vibrations $\nu + \delta$(Fe–O–Fe) have the largest contributions to the strong band near 552 cm^{-1} (Kolev *et al.*, 2003; Galuskina *et al.*, 2014; Gfeller *et al.*, 2015).

Table 1. Chemical composition of minerals of khesinite–dorrite series from Negev Desert.

	1			2			3			4	
No/Fig.	IS58/Fig. 2a			IS67/Fig. 2b			IS120a			IS74/Fig. 4a	
wt.%	n = 11	s.d.	Range	n = 11	s.d.	Range	n = 12	s.d.	Range	n = 5	s.d.
TiO_2	1.39	0.39	0.69–2.15	0.22	0.17	0.03–0.62	0.30	0.16	0.05–0.51	0.42	0.12
SiO_2	8.29	0.44	7.71–9.17	7.55	0.75	6.36–9.04	5.75	0.39	5.00–6.52	5.62	0.45
Fe_2O_3	63.44	1.45	60.93–65.76	67.40	2.87	64.18–72.32	68.69	1.43	65.88–71.38	50.95	0.46
Cr_2O_3	0.52	0.18	0.15–0.72	0.16	0.30	0–0.81	2.44	1.30	0.12–4.41	0.69	0.13
Al_2O_3	6.61	1.52	3.89–8.88	5.82	1.11	4.02–7.93	5.71	0.47	5.01–6.56	24.13	1.11
CaO	14.21	0.44	13.38–14.82	14.44	0.35	13.73–14.95	14.80	0.40	14.15–15.73	13.37	0.09
CuO	n.d.			0.34	0.19	0–0.65	n.d.			n.d.	
NiO	0.84	0.15	0.65–1.13	0.26	0.16	0.07–0.63	0.86	0.14	0.64–1.22	n.d.	
FeO	0.36			0.64							
MnO	0.57	0.10	0.45–0.80	0.18	0.29	0–0.81	0.28	0.04	0.17–0.34	0.07	0.02
MgO	3.41	0.42	2.87–4.12	2.20	0.76	1.58–3.72	1.13	0.14	0.86–1.30	3.63	0.25
Total	99.64			99.21			99.96			98.88	
				Calculated on 40 O							
Ca/A	***4***			***4***			***4***			***4***	
Ca	0.898			1.077			1.244			0.320	
Mg	0.849			0.697			0.557			1.632	
Mn^{2+}	0.155			0.050			0.078			0.018	
Fe^{2+}	0.098			0.176							
Ni							0.121				
M'	***2***			***2***			***2***			***1.97***	
Mg	0.786			0.379							
Cu^{2+}				0.084							
Ni^{2+}	0.217			0.069			0.108				
Fe^{3+}	8.528			9.372			9.223			9.831	
Cr^{3+}	0.132			0.042			0.638			0.164	
Ti^{4+}	0.336			0.054			0.075			0.095	
M	***10***			***10***			***10.044***			***10.090***	
Fe^{3+}	6.827			7.272			7.873			1.730	
Al	2.506			2.251			2.226			8.575	
Si	2.667			2.478			1.902			1.695	
T	***12***			***12***			***12***			***12***	

Note: Fe^{2+}/Fe^{3+} ratio calculated from stoichiometry.

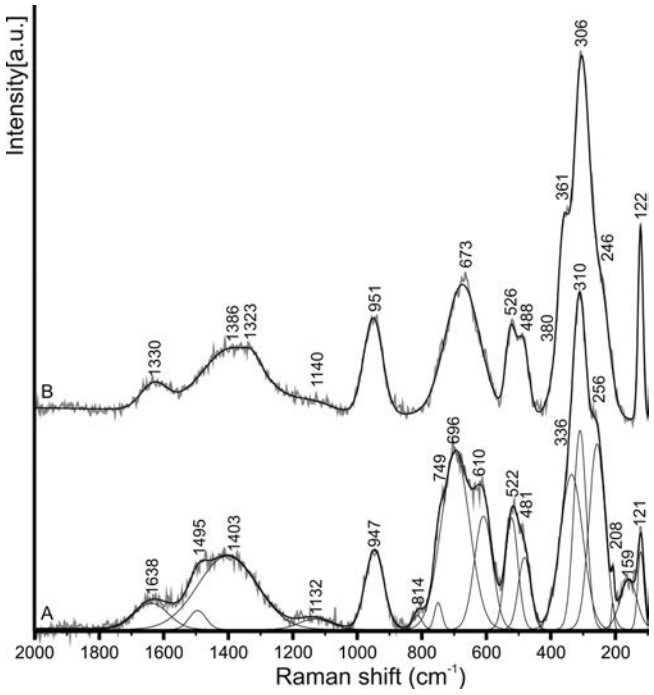

Fig. 3. The Raman spectra of khesinite (spectra A and B correspond to the A and B points shown in Fig. 2).

5. Crystal structure

Since khesinite is isostructural with rhönite and other minerals of the sapphirine supergroup (Bonaccorsi *et al.*, 1990; Grew *et al.*, 2008), the structure was first refined in the conventional cell setting $a = 9.061$, $b = 10.019$, $c = 10.536$ Å, $\alpha = 64.15$, $\beta = 84.24$, $\gamma = 65.64°$. The crystal was found to display 50:50 twinning. The twin components are related by a two-fold rotation about [1 1 0]* in agreement with the observations of Gasparik *et al.* (1999) for this structure type. De-twinning was achieved by application of the program Bruker Cell_Now. The final structure refinement was performed in the customary setting: $a = 10.5363(1)$, $b = 10.9242(2)$, $c = 9.0612(1)$ Å, $\alpha = 106.340(1)$, $\beta = 95.765(1)$, $\gamma = 124.373(1)°$.

Starting coordinates and site labelling were adopted from Cannillo *et al.* (1971), modified according to the chemical composition of khesinite. Details of data collection and structure refinement are given in Tables 2–4, anisotropic displacement parameters and the calculated powder diffraction pattern in Tables S2 and S3 of the Supplementary Material. Due to the similarity of Si and Al scattering factors, decision of using either Si or Al occupancy for tetrahedral sites was based on bond lengths. Thus in the final refinement, occupancy of *T*1 and *T*4 was refined with Si and Fe scattering factors, whereas occupancies of all other tetrahedral sites were refined with Al and Fe.

Only the tetrahedral site *T*4 is dominated by Si while bond lengths suggest that *T*1 has about 70% (Al + Si) with additional 30% Fe. These sites are the only tetrahedral sites in the structure bonded to three additional tetrahedra (Fig. 4), that is, the most polymerized *T* sites. The *T*2 and *T*3 sites, also members of the chains (Fig. 4), are occupied by about equal amounts of Al + Si and Fe^{3+}, and *ca.* 30% (Al + Si) and 70% Fe^{3+}, respectively. The *T*5 and *T*6 tetrahedra laterally attached to the chains are dominated (>95%) by Fe^{3+} (Fig. 4b). The Ca1 and Ca2 sites have 6 + 1 coordination by O. The octahedrally coordinated *M*1 to *M*7 sites are dominated by Fe^{3+} except the largest site *M*5, at which excess 0.45 Ca (according to results of chemical analyses) was fixed, and the remaining scattering power was modelled with Mg and Fe scattering factors. *M*1, *M*2, *M*3 and *M*7 have >95% Fe, whereas the occupancy of *M*6 converged to 77% Fe and 23% Mg.

Table 2. Parameters for X-ray data collection and structure refinement for khesinite.

Crystal data	
Unit-cell dimensions (Å)	$a = 10.5363(1)$ Å $b = 10.9242(2)$ Å $c = 9.0612(1)$ Å $\alpha = 106.340(1)°$ $\beta = 95.765(1)°$ $\gamma = 124.373(1)°$
Space group	$\overline{P}$
Volume (Å^3)	780.54(2)
Z	1
Chemical formula	$Ca_4(Fe,Mg)_{12}(Fe,Si,Al)_{12}O_{40}$
Intensity measurement	
Crystal shape	Prism
Crystal size (mm)	0.06 × 0.06 × 0.15
Diffractometer	APEX II SMART
X-ray radiation	Mo*K*α
X-ray power	50 kV, 30 mA
Monochromator	Graphite
Temperature	293 K
Detector to sample distance	5.95 cm
Measurement method	Phi and Omega scans
Radiation width	0.5°
Time per frame	60 s
Max. θ° range for data collection	41.45
Index ranges	$-19 \le h \le 0$ $-16 \le k \le 20$ $-16 \le l \le 16$
No. of measured reflections	23,540
No. of unique reflections	8795
No. of observed reflections ($I > 2\sigma(I)$)	7230
No. of parameters used in refinement	321
*R*σ	0.0441
*R*1, $I > 2\sigma(I)$	0.0350
*R*1 all data	0.0462
*wR*2 on (F^2)	0.0932
GooF	1.040

Table 3. Atom fractional coordinates and equivalent isotropic displacement parameters (Å^2) for khesinite.

Site	*x*	*y*	*z*	U_{eq}	Occupancy	epfu
Fe1	0	0	0.5	0.00750(9)	1 Fe	26
Fe2	0	0.5	0	0.00729(9)	1 Fe	26
Fe3	0.30869(5)	0.85081(5)	0.17035(5)	0.00724(7)	1 Fe	26
Fe4	0.77995(5)	0.82911(5)	0.15123(5)	0.00791(7)	1 Fe	26
Mg5	0.09567(8)	0.93956(9)	0.05401(10)	0.00842(16)	0.036(4) Fe, 0.514(4) Mg, 0.45 Ca	16.104
Fe6	0.59574(5)	0.94383(6)	0.05847(6)	0.00659(10)	0.767(4) Fe, 0.232(4) Mg	22.726
Fe7	0.99695(4)	0.74279(4)	0.25809(5)	0.00635(9)	0.949(4) Fe, 0.051(4) Mg	25.286
Ca1	0.20555(6)	0.62478(6)	0.38820(7)	0.00862(9)	1	40
Ca2	0.66315(5)	0.61437(6)	0.37416(7)	0.00844(9)	1	40
T1	0.47016(7)	0.23549(7)	0.33554(8)	0.00764(15)	0.750(4) Si, 0.294(4) Fe	18.144
T2	0.96999(6)	0.22859(6)	0.34863(7)	0.00633(13)	0.512(4) Al, 0.488(4) Fe	19.344
T3	0.78349(5)	0.34868(5)	0.23697(6)	0.00618(11)	0.289(4) Al, 0.711(4) Fe	22.243
T4	0.26889(8)	0.33892(8)	0.22820(9)	0.00711(18)	0.940(4) Si, 0.060(4) Fe	14.72
T5	0.63996(4)	0.94782(4)	0.43432(5)	0.00592(9)	0.037(4) Al, 0.963(4) Fe	25.519
T6	0.36453(4)	0.56579(4)	0.04809(5)	0.00617(9)	0.046(4) Al, 0.954(4) Fe	25.402
O1	0.3483(3)	0.0555(3)	0.1588(3)	0.0115(3)	1	
O2	0.8333(2)	0.0464(2)	0.1652(3)	0.0117(4)	1	
O3	0.5390(2)	0.9595(2)	0.2649(3)	0.0098(3)	1	
O4	0.0178(2)	0.9400(2)	0.2720(3)	0.0084(3)	1	
O5	0.2390(2)	0.8609(2)	0.3729(3)	0.0075(3)	1	
O6	0.7622(2)	0.8762(2)	0.3768(3)	0.0079(3)	1	
O7	0.5140(2)	0.2115(2)	0.5087(3)	0.0125(4)	1	
O8	0.9565(2)	0.7873(2)	0.4759(3)	0.0093(3)	1	
O9	0.8804(3)	0.3241(3)	0.3904(3)	0.0132(4)	1	
O10	0.3714(3)	0.3245(3)	0.3657(3)	0.0137(4)	1	
O11	0.6430(2)	0.1596(2)	0.0516(3)	0.0091(3)	1	
O12	0.1542(3)	0.1713(3)	0.0584(3)	0.0126(4)	1	
O13	0.5551(2)	0.7342(2)	0.0387(3)	0.0095(3)	1	
O14	0.0654(2)	0.7267(2)	0.0601(3)	0.0086(3)	1	
O15	0.2382(2)	0.6247(2)	0.1218(3)	0.0074(3)	1	
O16	0.7550(2)	0.6269(2)	0.1422(3)	0.0080(3)	1	
O17	0.4091(2)	0.5005(2)	0.2034(3)	0.0107(3)	1	
O18	0.9504(2)	0.5253(2)	0.2128(3)	0.0086(3)	1	
O19	0.1516(3)	0.3699(3)	0.3100(3)	0.0139(4)	1	
O20	0.6604(3)	0.3892(3)	0.3329(3)	0.0149(4)	1	

6. Khesinite and other ferrites in pyrometamorphic rocks of the Hatrurim Complex

In order to obtain the information needed to address questions concerning the crystal chemistry and genesis of khesinite, we have supplemented data obtained on the holotype khesinite with information on the morphology, chemical composition of khesinite and associated minerals from other localities in the Hatrirum Complex. Minerals of the khesinite–dorrite series are widely distributed in fine-grained gehlenite–flamite hornfelses and in thin veins and lenses of paralavas, the thickness of which ranges from 1 to 5 cm and very rarely reaches 20–30 and more cm in width.

A paralava sample (no. IS67), which is characterized by a mineral composition similar to that in the holotype specimen (no. IS58), was collected at several hundred metres distance from it in the Negev Desert. In that sample (IS67), khesinite is confined to fine-grained, iron-enriched areas, a few millimetres across, interstitial between large crystals of gehlenite, rankinite, schorlomite and pseudo-wollastonite. In that sample, khesinite (Fig. 2b; Table 1, analysis 2, mean of 11 analyses and Table 5, analysis 3) usually forms fine reaction rims on Ni-bearing magnesioferrite (Table 5, analysis 2) with relics of Cr-bearing hematite (Table 5, analysis 1) and was overgrown by andradite (Table 5, analysis 5). Khesinite in paralava is commonly associated with barioferrite (Table 5, analysis 4) and unusual Si- and Fe^{3+}-bearing perovskite (Table 5 , analysis 6). Khesinite in sample IS67 has the simplified formula (calculated on the basis of the mean analysis) ~ $Ca_4(Fe^{3+}_{9.50}Mg_{1.5}Ca)_{\Sigma 12}[(Fe^{3+}_{7.5}Al_2Si_{2.5})_{\Sigma 12}O_{40}]$, which is close to the holotype khesinite composition, differing only in its higher Cu content (Table 1, analyses 1, 2). More than 70 analyses of khesinite from paralavas of the Negev Desert (two sections cut from specimens no. IS58, IS67) were used for the construction of the Fe^{3+}–Al–Si classification diagram for the tetrahedral cations. These analyses plot in the khesinite area between the lines Si = 1 apfu and Si = 3 apfu (Fig. 5).

In gehlenite–flamite hornfels (specimen JB3, Jabel Harmun locality), khesinite and magnesioferrite form crusts on the walls of small channels a few millimetres in

Table 4. Selected interatomic distances (Å) in khesinite.

Atom	–Atom	Dist. (Å)		Atom	–Atom	Dist. (Å)
Fe1	O8	2.0370(18)	×2	Ca1	O7	2.3113(19)
	O6	2.0287(18)	×2		O9	2.338(2)
	O4	2.047(2)	×2		O19	2.367(2)
	Mean	2.038			O18	2.409(2)
Fe2	O15	2.0273(18)	×2		O5	2.4451(18)
	O18	2.0334(18)	×2		O15	2.472(2)
	O14	2.0353(19)	×2		O20	2.855(2)
	Mean	2.032			Mean	2.457
Fe3	O3	1.947(2)		Ca2	O17	2.331(2)
	O15	2.0240(18)			O20	2.364(2)
	O5	2.042(2)			O10	2.387(2)
	O14	2.0506(19)			O16	2.407(2)
	O1	2.0669(19)			O6	2.4203(18)
	O11	2.112(2)			O8	2.4142(19)
	Mean	2.040			O10	2.882(2)
Fe4	O13	1.9679(19)			Mean	2.458
	O6	2.018(2)		T1	O7	1.722(2)
	O16	2.0477(18)			O1	1.744(2)
	O4	2.0540(19)			O20	1.752(2)
	O2	2.0681(19)			O10	1.776(2)
	O12	2.087(2)			Mean	1.749
	Mean	2.040		T2	O9	1.755(2)
Mg5	O1	2.145(2)			O2	1.794(2)
	O12	2.145(2)			O8	1.794(2)
	O14	2.1798(19)			O19	1.809(2)
	O4	2.213(2)			Mean	1.788
	O2	2.206(2)		T3	O9	1.812(2)
	O12	2.228(2)			O20	1.815(2)
	Mean	2.186			O18	1.8291(18)
Fe6	O3	2.011(2)			O11	1.837(2)
	O13	2.0263(19)			Mean	1.823
	O2	2.048(2)		T4	O17	1.6416(19)
	O11	2.062(2)			O19	1.645(2)
	O1	2.112(2)			O12	1.650(2)
	O11	2.1376(19)			O10	1.666(2)
	Mean	2.066			Mean	1.651
Fe7	O14	1.999(2)		T5	O3	1.855(2)
	O4	2.0034(18)			O7	1.8474(19)
	O18	2.0373(18)			O5	1.880(2)
	O8	2.043(2)			O6	1.8934(19)
	O5	2.0614(19)			Mean	1.869
	O16	2.0675(19)		T6	O13	1.8375(18)
	Mean	2.040			O16	1.876(2)
					O17	1.8757(19)
					O15	1.8807(18)
					Mean	1.867

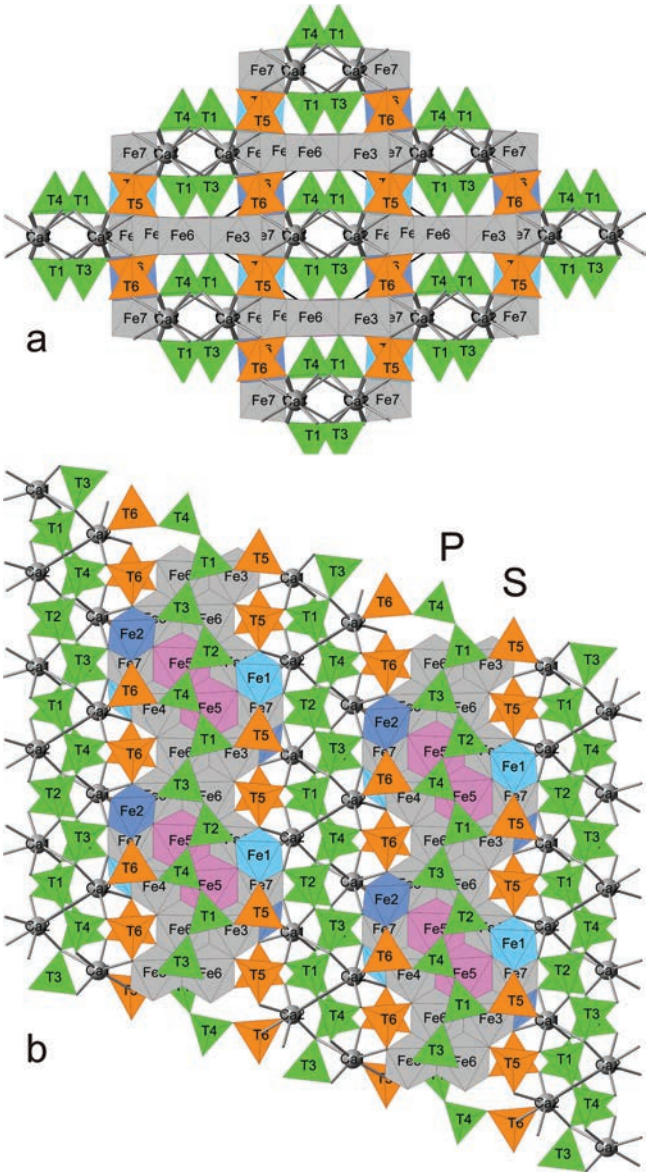

Fig. 4. The khesinite structure, projections on (1 0 0) (a) and (2 3 3) (b). Tetrahedral and octahedral layers are distinguished. In tetrahedral layers pyroxene chains (P, green triangles) extend along [1 0 0] and are formed by different types of tetrahedra: *T*4 (mean distance M–O = 1.65 Å) is occupied by Si; *T*1 (1.75 Å) – Si + Al; *T*2 (1.79 Å) – Al + Fe^{3+}; *T*3 (1.82 Å) – Fe^{3+} + Al. The spinel module is composed by trimers: *T*6–*Fe*2–*T*6 or *T*5–*Fe*1-–*T*5. All sites are predominantly occupied by Fe^{3+}, which is confirmed by mean M–O distances: tetrahedra (orange) *T*5 = 1.87 Å and *T*6 = 1.87 Å, octahedra (blue) *Fe*1 = 2.04 Å and *Fe*2 = 2.03 Å.

diameter (Fig. 6a, Table 6, analysis 2) and on rims of magnesioferrite grains (Fig. 6b, Table 7, analyses 1, 3). These magnesioferrite grains contain platy inclusions of a potentially new mineral – the Ca-analogue of barioferrite, close to $CaFe_{12}O_{19}$ in composition (Table 7, analysis 2). Khesinite and other ferrites also fill fine cracks in gehlenite–flamite hornfels from Jabel Harmun and form reaction rims on magnesioferrite (Fig. 6c–f; specimens JB1, JBB16, JBB17, JB4a, Table 6, analyses 3–5). Khesinite is also found with barioferrite and its Ca-analogue (Fig. 6d–f; Table 7, analyses 5, 11, 12, 14). Fe^{3+}-bearing gehlenite or schorlomite forms rims on khesinite (Fig. 6d; Table 7, analysis 10). Khesinite replacing magnesioferrite shows up to 10.2 wt.% Cr_2O_3 (Table 6, analyses 1, 5; Table 7, analysis 15). In hornfels from Jabel Harmun, the main rock-forming minerals are flamite and gehlenite, where flamite is an analogue of α-Ca_2SiO_4 stabilized by K, Na, P impurities and recently described as a new mineral (Sokol *et al.*, 2015; Gfeller *et al.*, 2015). In hornfels from the Jabel Harmun, polysynthetically twinned grains of flamite occur widely as well as flamite

Table 5. Compositions of minerals in the Fe^{3+}-bearing assemblage in paralava from Negev (IS67).

Analysis no.	1	2	3	4	5	6
Fig. 2b no.		1	2		3	
Mineral	Hem	Mgf	Khs	Bfr	Adr	Prv
Weight%						
V_2O_5	n.d.	n.d.	n.d.	n.d.	0.57	n.d.
TiO_2	0.24	0.00	0.32	3.02	0.40	46.35
SiO_2	n.d.	n.d.	9.04	n.d.	34.78	2.72
Fe_2O_3	97.47	68.20	62.88	79.43	29.51	7.99
Cr_2O_3	1.30	1.88	0.81	0.07	0.06	0.21
Al_2O_3	0.47	1.71	6.09	1.87	1.05	0.35
BaO	n.d.	n.d.	n.d.	12.99	n.d.	n.d.
SrO	n.d.	0.15	0.09	0.47	n.d.	0.34
NiO	n.d.	9.75	0.63	0.25	n.d.	n.d.
CuO	n.d.	2.24	0.42	0.21	n.d.	n.d.
ZnO	n.d.	1.59	n.d.	0.28	n.d.	n.d.
MnO	0.15	0.83	0.24	0.23	n.d.	n.d.
FeO	n.d.	4.48	1.93	0.08	0.71	n.d.
CaO	0.21	0.37	14.17	0.61	32.86	41.33
MgO	0.05	7.89	2.48	0.65	0.02	n.d.
Total	99.89	99.09	99.10	100.16	99.96	99.29
Calc. on	3 O	4 O	40 O	19 O	12 O	3 O
Ca			3.982	0.033	2.972	0.999
Ba				0.918		0.004
Sr			0.018	0.049		
Fe^{2+}					0.025	
Mg					0.003	
Sum *X*			*4*	*1*	*3*	*1.003*
Al						0.009
Cr^{3+}	0.027	0.054	0.210	0.010	0.004	0.004
Fe^{3+}	1.944	0.874	8.687	9.173	1.874	0.136
Si						0.061
Ti	0.005		0.079	0.409	0.025	0.787
Ca	0.006	0.014	0.961	0.085		
Sr		0.003				
Mg	0.002	0.429	1.202	0.175		
Ni^{2+}		0.286	0.166	0.036		
Cu^{2+}		0.062	0.104	0.029		
Zn		0.043		0.038		
Mn^{2+}	0.003	0.025	0.066	0.036		
Fe^{2+}		0.137	0.525	0.011	0.025	
Al	0.015	0.073			0.072	
Sum *M*	*2.002*	*2*	*12*	*10.002*	*2*	*1*
Al			2.338	0.398	0.032	
Fe^{3+}		1.000	6.721	1.602		
Si			2.943		2.936	
V^{5+}					0.032	
Sum *T*		*1*	*12.002*	*2*	*3*	

Note: Fe^{2+}/Fe^{3+} ratio calculated from stoichiometry. Abbreviations: Hem – hematite, Mgf – magnesioferrite, Khs – khesinite, Brf – barioferrite, Adr – andradite, Prv – perovskite.

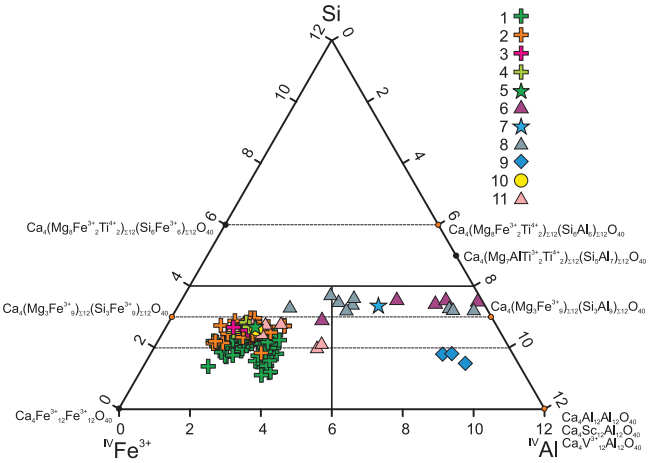

Fig. 5. Tetrahedral sites composition projected in the Fe^{3+}–Al–Si diagram. 1–4 Khesinite: 1 – holotype (Table 1, analysis 1); 2 – paralava, Negev; 3 – gehlenite hornfels, Negev Desert and Judean Mts; 4 – esseneite–melilite paralava, Zelénky, Czech Republic (Záček *et al.*, 2015); 5 – gehlenite hornfels, Nabi Musa (Sokol *et al.*, 2011); 6–8 Dorrite: 6 – gehlenite hornfels, Negev; 7, 8 (mean analysis) – holotype (Cosca *et al.*, 1988); 9 – "Fe^{3+} reach melilite" (Foit *et al.*, 1987); 10 – "malachovite" (Chesnokov *et al.*, 2008); 11 – "anthropogenic khesinite" (Gatel *et al.*, 2015).

replaced by a symplectite intergrowth of silicocarnotite and rankinite, where rankinite is replaced by Ca-hydrosilicates (Galuskin *et al.*, 2016). Silococarnotite is replaced by khesinite in decomposed flamite grains in close vicinity to magnesioferrite grains with khesinite rims (Fig. 6f). Early silicates have been altered by widespread secondary hydration and carbonatization of flamite–gehlenite hornfels.

Isolated aggregates of platy khesinite crystals with magnesioferrite relics distributed along cracks filled by hydrosilicates and thaumasite were detected in gehlenite–flamite hornfels from the Ma'ale Adummim locality, 12-km east of Jerusalem (Table 6, analysis 6) and also within Gurim anticline in the Negev Desert (Table 1, analysis 3).

Khesinite compositions from gehlenite–flamite rocks plot between the lines Si = 2 apfu and Si = 3 apfu in the classification diagram Fe^{3+}–Al–Si (Fig. 5).

Dorrite in very limited quantity was found in altered flamite–gehlenite hornfels in Gurim anticline, Negev Desert (Fig. 7a; Table 8, analysis 4), where primary spinel is intermediate in composition between magnesioferrite and spinel (Table 8, analysis 1). Dorrite analyses plot below the line Si = 2 on the classification diagram (Fig. 5). Dorrite forms rims on spinel grains, more rarely on brownmillerite and shulamitite (Table 8, analyses 2, 3) as well as on a potentially new mineral with composition ~$Ca_2Mg_2Fe_{10}(Al,Fe)_4O_{25}$ (Fig. 7a; Table 8, analysis 3), which is probably an analogue of the synthetic ferrite (CFF) with formula $Ca_4Fe_{14}O_{25}$. The natural analogue of the CFF phase was also detected as rims on spinel in hornfels from the Jabel Harmun (Fig. 7b; Table 8, analyses 7, 8).

7. Discussion

The structure of minerals of the rhönite group is traditionally thought to consist of alternating octahedral and tetrahedral layers (Fig. 4a). Octahedral walls are formed by *M*3–*M*7 octahedra, which are mainly occupied by Fe^{3+}, excluding the *M*5 octahedron occupied by Mg and *Ca*1and *Ca*2 polyhedra (configuration 6 + 1).

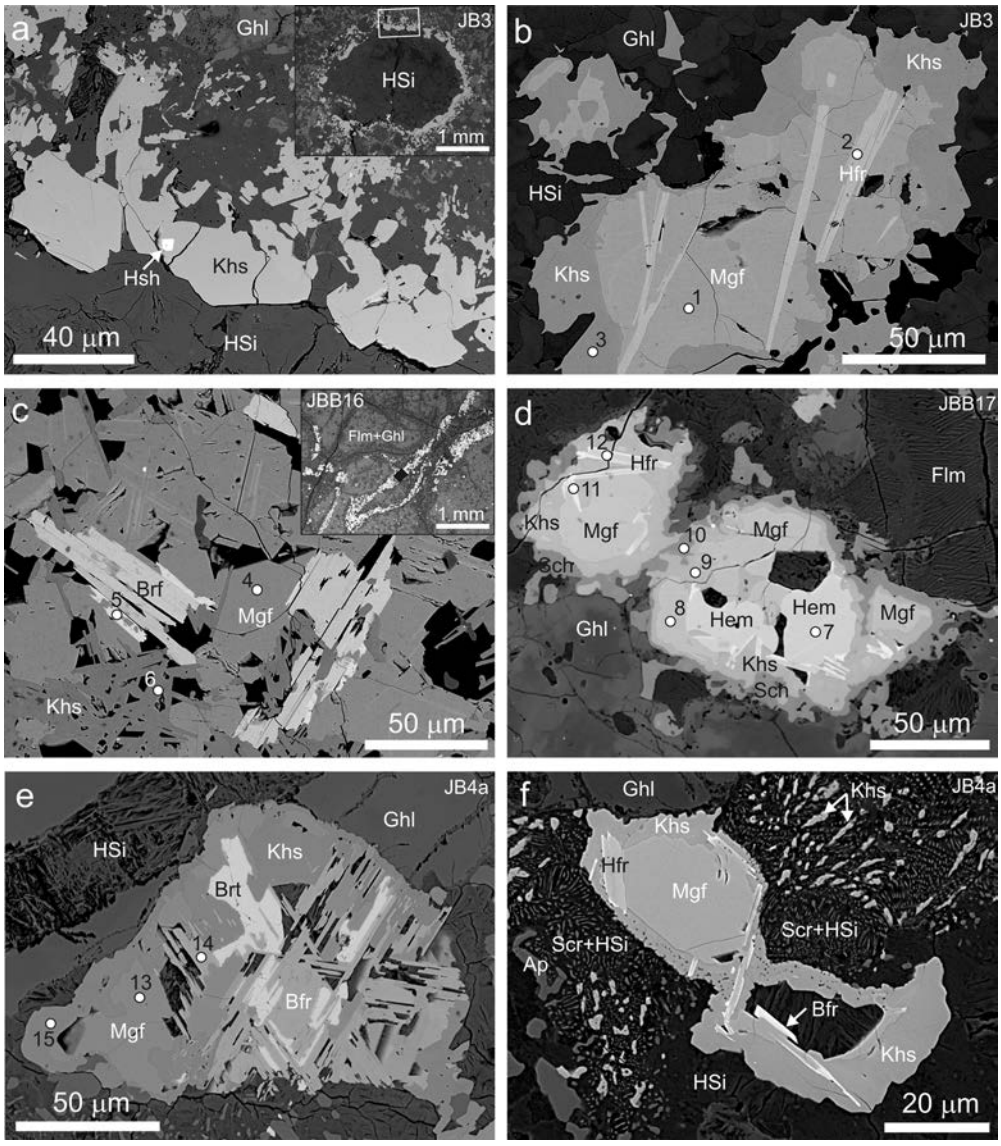

Fig. 6. (a and b) Specimen no. JB3: a magnesioferrite and khesinite incrusting walls of rounded channels in flamite–gehlenite hornfels (channel is shown in inset, magnified fragment is outlined by frame); bright spot in khesinite is a hashemite $BaCrO_4$ grain. (b) Khesinite rims on magnesioferrite with inclusions of "calcioferrite". (c) Specimen no. JBB16: khesinite together with magnesioferrite and barioferrite fill thin cracks in flamite–gehlenite hornfels as shown in inset, black rectangle shows magnified fragment in (c). (d) Specimen no. JBB17: zoned aggregate of hematite–magnesioferrite–khesinite–schorlomite with "calcioferrite" inclusions, which is replaced by barioferrite. On the right upper corner partially altered flamite with characteristic polysynthetic twinning is visible. (e and f) Altered magnesioferrite grains with khesinite rims and "hexaferrite" inclusions: (e) barite forms in empty spaces in magnesioferrite; (f) symplectite of silicocarnotite and rankinite (replaced by Ca-hydrosilicates) are well visible. Some part of silicocarnotite is replaced by khesinite. BSE images. Points of analyses given in Tables 6 and 7 are shown in Fig. 6. Adr – andradite, Bfr – barioferrite, Brt – barite, Cal – calcite, Ghl – gehlenite, Hsh – hashemite, HSi – hydrosilicates, Khs – khesinite, Mgf – magnesioferrite, Ap – fluorapatite, Hfr – "Ca hexaferrite", Flm – flamite, Scr – silicocarnotite, Hem – hematite, Sch – schorlomite.

Pyroxene chains (P) extend parallel to the *X* axis in the tetrahedral layer, between which are located spinel modules (S), formed by linear *T*5–*Fe*1–*T*5 and *T*6–*Fe*2–*T*6 trimers (Fig. 4b; Zvyagin, 1997; Merlino & Pasero, 1997). This arrangement corresponds to the polysome ⟨SP⟩ (Fig. 4b) reported in the synthetic phases of the SFCA type, which are close in composition and structure to khesinite (Hamilton *et al.*, 1989; Mumme *et al.*, 1998; Sugiyama *et al.*, 2005; Liles *et al.*, 2016). Most minerals of the sapphirine supergroup are also ⟨SP⟩ polysomes (Grew *et al.*, 2008). Investigations of synthetic Ca-ferrites showed that there are other modular structures formed by S- and P-modules such as ⟨SSP⟩ for SFCA-I with composition $Ca_{6.36}Fe^{3+}_{29.32}Al_{2.68}Fe^{2+}_{0.82}O_{56}$ (Mumme *et al.*, 1998) and ⟨SSPSP⟩, which corresponds to ⟨SSP⟩ + ⟨SP⟩, for the SFCA-II phase $Ca_{10.2}Al_{18.6}Fe^{3+}_{37.4}Fe^{2+}_{1.8}O_{96}$ (Mumme, 2003).

The structural formula of minerals of the dorrite–khesinite series can be written as follows: $^{VII}(A1_2A2_2)_{\Sigma4}{}^{VI}(M1M2M3_2M4_2M5_2M6_2M7_2)_{\Sigma12}O_4$ $[(T1_2T2_2T3_2T4_2T5_2T6_2)_{\Sigma12}O_{36}]$,

Table 6. Chemical composition of khesinite from Judean Desert.

	1			2			3			4			5			6		
No.	JB1			JB3			JBB16			JBB17			JB4a			MA2A		
wt.%	*n* = 27	s.d.	Range	*n* = 27	s.d.	Range	*n* = 13	s.d.	Range	*n* = 23	s.d.	Range	*n* = 34	s.d.	Range	*n* = 26	s.d.	Range
TiO_2	0.45	0.05	0.33–0.54	0.32	0.08	0.18–0.48	0.65	0.04	0.57–0.70	0.76	0.21	0.42–1.13	0.50	0.17	0.09–0.76	0.95	0.12	0.70–1.12
SiO_2	6.58	0.44	5.22–7.44	6.98	0.87	4.13–8.12	5.12	0.55	4.17–5.73	5.21	0.96	3.30–6.51	6.26	1.15	4.53–8.77	5.35	0.39	4.60–6.37
Fe_2O_3	64.03	2.90	58.33–68.82	69.16	2.34	67.06–75.48	68.43	1.32	66.84–70.77	69.24	1.84	66.23–72.67	65.86	4.67	52.59–71.03	67.87	1.16	65.56–70.24
Cr_2O_3	4.20	1.53	2.03–6.93	0.56	0.13	0.29–0.80	0.72	0.40	0.16–1.29	0.30	0.27	0.03–1.03	2.28	2.82	0.33–10.20	0.66	0.13	0.48–0.98
Al_2O_3	6.58	1.12	3.93–8.98	5.68	0.64	4.31–6.73	7.91	0.37	7.41–8.69	7.96	1.38	5.13–9.51	7.45	1.44	2.58–9.66	7.20	0.51	5.91–7.93
CaO	14.72	0.25	14.16–15.21	14.44	0.38	13.37–15.03	14.23	0.34	13.74–14.66	13.92	0.55	12.61–14.78	14.23	0.39	13.49–15.07	14.15	0.31	13.58–14.77
CuO	0.14	0.05	0.03–0.21	n.d.			n.d.			n.d.			0.41	0.15	0.17–0.79	0.08	0.04	0–0.16
ZnO	n.d.			n.d.			0.20	0.10	0.02–0.36	n.d.			n.d.			n.d.		
NiO	0.33	0.11	0.13–0.55	0.28	0.09	0.07–0.52	n.d.			0.10	0.04	0–0.18	0.14	0.08	0–0.31	0.14	0.03	0.10–0.22
FeO	n.d.			0.35			0.08			n.d.			n.d.			n.d.		
MnO	0.18	0.04	0.07–0.27	0.14	0.05	0.07–0.22	n.d.			0.11	0.06	0–0.23	0.20	0.07	0–0.33	0.09	0.04	0–0.14
MgO	2.03	0.19	1.66–2.36	2.27	0.28	1.35–2.64	1.51	0.14	1.24–1.71	2.29	0.35	1.67–3.41	2.19	0.69	0–3.34	2.18	0.24	1.70–2.68
Total	99.24			100.18			98.87			99.90			99.51			98.67		
							Calculated on 40 O											
Ca/X	*4*			*4*			*4*			*4*			*4*			*4*		
Ca	1.169			1.044			1.040			0.863			0.975			1.016		
Fe^{2+}				0.095			0.021											
Mg	0.781			0.822			0.744			1.106			1.025			0.959		
Mn^{2+}	0.050			0.039						0.031			0.055			0.025		
Zn							0.049											
Fe^{3+}							0.146											
M′	*2*			*2*			*2*			*2*			*2*			*2*		
Fe^{3+}	8.490			9.424			9.650			9.750			9.079			9.473		
Cr^{3+}	1.088			0.144			0.188			0.077			0.588			0.173		
Mg	0.211			0.281						0.008			0.040			0.116		
Ti^{4+}	0.111			0.078			0.162			0.187			0.123			0.236		
Cu^{2+}	0.035												0.101			0.020		
Ni	0.087			0.073						0.027			0.037			0.037		
M	*10.022*			*10*			*10*			*10.049*			*10.022*			*10.055*		
Si	2.157			2.276			1.693			1.700			2.043			1.770		
Fe^{3+}	7.302			7.542			7.226			7.241			7.093			7.423		
Al	2.542			2.182			3.082			3.059			2.865			2.807		
T	*12*			*12*			*12*			*12*			*12*			*12*		

Note: Fe^{2+}/Fe^{3+} ratio calculated from stoichiometry.

Table 7. Composition of ferrites from flamite–gehlenite hornfels from Jabel Harmun, Judean Mts.

No.	JB3			JBB16			JBB17						JB4A		
Fig.	3B			3C			3D						3E		
Mineral	Mgf	Hfr	Khs	Mgf	Bfr	Ksh	Hem	Mgf	Khs	Sch	Brf	Hfr	Mgf	Bfr	Khs
wt.%	1	2	3	4	5	6	7	8	9	10	11	12	13	14	15
TiO_2	n.d.	0.57	0.33	0.07	1.48	0.70	1.00	0.12	0.43	13.37	1.99	2.67	n.d.	2.48	0.46
SiO_2	n.d.	n.d.	7.31	n.d.	n.d.	5.40	n.d.	n.d.	7.26	22.85	0.23	0.05	0.03	n.d.	6.91
Fe_2O_3	70.21	89.81	67.57	68.91	81.63	67.75	95.70	69.41	67.84	30.44	80.29	85.15	64.65	78.60	59.65
Cr_2O_3	1.54	1.90	0.42	0.13	n.d.	1.02	1.84	2.03	0.92	0.34	1.62	2.07	7.74	1.91	5.74
Al_2O_3	1.28	1.45	6.01	2.89	2.07	7.98	0.67	1.64	6.13	1.02	1.64	1.90	1.85	1.68	8.77
BaO	n.d.	n.d.	n.d.	0.16	11.64	n.d.	n.d.	n.d.	n.d.	n.d.	10.54	0.97	0.19	10.81	n.d.
SrO	n.d.	n.d.	n.d.	n.d.	n.d.	n.d.	n.d.	n.d.	n.d.	n.d.	0.23	0.25	0.25	0.46	0.18
CoO	n.d.	n.d.	n.d.	n.d.	n.d.	n.d.	n.d.	n.d.	n.d.	n.d.	n.d.	n.d.	0.16	n.d.	n.d.
NiO	4.32	0.16	0.24	2.25	n.d.	0.08	n.d.	2.41	n.d.	n.d.	0.16	0.28	3.55	0.20	0.23
CuO	0.65	n.d.	n.d.	1.07	n.d.	n.d.	n.d.	2.61	0.22	n.d.	0.18	0.25	4.03	0.17	0.32
ZnO	0.19	n.d.	n.d.	5.95	0.31	0.33	n.d.	0.51	0.13	n.d.	n.d.	0.14	1.18	n.d.	n.d.
MnO	0.39	0.19	0.21	0.16	n.d.	n.d.	n.d.	0.37	0.15	n.d.	0.29	0.26	0.43	0.16	n.d.
FeO	10.53	0.31	0.30	6.62	n.d.	0.03	n.d.	7.65	0.19	n.d.	n.d.	n.d.	2.84	n.d.	n.d.
CaO	0.93	5.52	15.22	0.59	0.95	14.34	0.17	0.85	14.71	32.34	2.22	5.47	0.55	1.20	14.54
MgO	9.09	0.32	1.92	9.59	0.30	1.59	0.35	10.83	2.44	n.d.	0.79	1.09	12.13	0.88	2.58
K_2O	n.d.	n.d.	n.d.	n.d.	0.07	n.d.	n.d.	n.d.	n.d.	n.d.	n.d.	0.14	n.d.	n.d.	n.d.
Na_2O	n.d.	n.d.	n.d.	n.d.	0.09	n.d.	n.d.	n.d.	n.d.	n.d.	0.05	n.d.	n.d.	n.d.	n.d.
Total	99.13	100.23	99.53	98.39	98.54	99.23	99.73	98.43	100.42	100.36	100.23	100.69	99.56	98.55	99.38
Calc. on	4 O	19 O	40 O	4 O	19 O	40 O	3 O	4 O	40 O	8 O	19 O	19 O	4 O	19 O	40 O
Na					0.032						0.017				
K					0.016							0.030			
Ca		0.986	4.000		0.122	4.000			4.000	3.034	0.228	0.883		0.231	3.966
Ba					0.830						0.731	0.063		0.765	
Sr											0.024	0.024		0.048	0.034
Mn^{2+}		0.026													
X		*1.012*	*4*		*1*	*4*			*4*	*3.034*	*1*	*1*		*1.044*	*4*
Ca	0.036		1.333	0.023	0.063	1.049	0.005	0.033	1.100		0.193	0.087	0.021		1.054
Ba				0.002									0.003		
Mg	0.488	0.080	0.938	0.515	0.081	0.781	0.014	0.577	1.177		0.209	0.269	0.634	0.237	1.241
Co													0.005		
Ni	0.125	0.022	0.063	0.065		0.021		0.069			0.023	0.037	0.100	0.029	0.059
Cu	0.018			0.029				0.070	0.054		0.024	0.031	0.107	0.023	0.078
Zn	0.005			0.162	0.043	0.082		0.014	0.032			0.018	0.031		
Mn^{2+}	0.012		0.058	0.005				0.011	0.041		0.043	0.036	0.013	0.025	
Fe^{2+}	0.317	0.044	0.081	0.200		0.008		0.229	0.050				0.083		
Al	0.054						0.021						0.076	0.358	
Cr^{3+}	0.044	0.251	0.107	0.004		0.265	0.038	0.057	0.235	0.024	0.227	0.271	0.215	0.273	1.462
Fe^{3+}	0.901	9.551	9.340	0.993	9.626	9.621	1.902	0.937	9.206	1.095	9.083	8.984	0.712	10.682	8.025
Ti^{4+}		0.071	0.080	0.002	0.203	0.173	0.020	0.003	0.105	0.881	0.265	0.332		0.337	0.112
M	*2*	*10.019*	*12*	*2*	*10.016*	*12*	*2*	*2*	*12*	*2*	*10.067*	*10.065*	*2*	*11.964*	*12.031*
Al		0.284	2.317	0.123	0.444	3.092		0.069	2.338	0.105	0.342	0.371			3.332
Fe^{3+}	1.000	1.715	7.291	0.877	1.556	7.133		0.931	7.313	0.911	1.617	1.621	0.997		6.442
Si			2.392			1.775			2.349	2.001	0.041	0.008	0.003		2.226
T	*1*	*2*	*12*	*1*	*2*	*12*		*1*	*12*	*3.017*	*2*	*2*	*1*		*12*

Note: Fe^{2+}/Fe^{3+} ratio calculated from stoichiometry. Abbreviations: Mgf – magnesioferrite, Hfr – hexaferrite, Khs – khesinite, Brf – barioferrite, Hem – hematite, Schr – schorlomite.

where seven-coordinated *A* sites are occupied by Ca, octahedral *M* sites by $Fe^{2+,3+}$, Mg, Ti^{4+}, Cr^{3+}, Ca and tetrahedral *T* sites by Si, Al and Fe^{3+}. This structural formula can be simplified to $A_4(M_{12})O_4[T_{12}O_{36}]$ in the sapphirine-supergroup classification. The formula $Ca_4(Mg_3Fe^{3+}{}_9)O_4[Si_3Al_8Fe^{3+}O_{36}]$ was proposed for holotype dorrite (Grew *et al.*, 2008). This formula does not correspond to a proper end-member crystal-chemical formula as more than two cations occupy the combined *M* sites and combined *T* sites (*cf.* Hawthorne, 2002). For holotype khesinite with the empirical formula $Ca_4(Fe^{3+}{}_{8.528}Mg_{1.635}Ca_{0.898}Ti^{4+}{}_{0.336}Ni^{2+}{}_{0.217}Mn^{2+}{}_{0.155}Cr^{3+}{}_{0.132}Fe^{2+}{}_{0.098})_{\Sigma 12}O_4[(Fe^{3+}{}_{6.827}Al_{2.506}Si_{2.667})_{\Sigma 12}O_{36}]$ (Table 1, analysis 1), we proposed by analogy with dorrite the crystal-chemical formula $Ca_4(Fe^{3+}{}_9Mg_3)O_4[(Fe^{3+}{}_9Si_3)O_{36}]$.

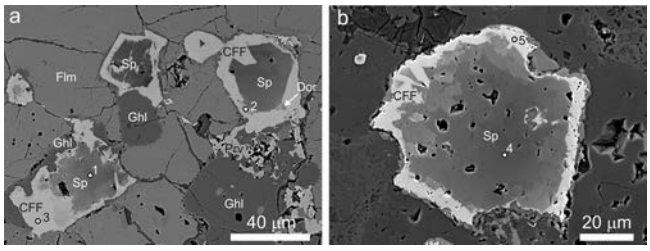

Fig. 7. Rims of CFF-type phase on spinel crystals from flamite–gehlenite hornfelses. (a) Specimen no. IS74A: rare dorrite grains are detected within rims. (b) Specimen no. IS104: Fe content in spinel grains increases towards margin, lighter spots are visible. BSE images. Ghl – gehlenite, Dor – dorrite, Sp – spinel-magnesioferrite, Flm – flamite, Prv – perovskite; CFF – CFF-type phase. Points of analyses given in Table 8 correspond to the numbers shown in the figures.

However, this formula also does not meet the formal requirements of an end-member formula. According to the dominant-valence rule, the empirical formula of khesinite might be simplified to $Ca_4(Fe^{3+}{}_{12})O_4[Fe^{3+}{}_{12}]O_{36}$ with combined *M* and *T* sites. This is the extreme approach applied by Ma and co-authors describing the new minerals warkite $Ca_4Sc_{12}O_4[Al_{12}O_{36}]$ (IMA2013-129) (Ma *et al.*, 2014), beckettite (IMA2015-001) $Ca_4V_{12}O_4[Al_{12}O_{36}]$ (Ma *et al.*, 2015) and addibischoffite (IMA2015-006) $Ca_4Al_{12}O_4[Al_{12}O_{36}]$ (Ma & Krot, 2015). Following this procedure, the dorrite formula would be simplified to $Ca_4(Fe^{3+}{}_{12})O_4[Al_{12}]O_{36}$, and the formula originally suggested for the species khesinite, $Ca_4(Fe^{3+}{}_9Mg_3)O_4(Fe^{3+}{}_9Si_3)O_{36}$ (Galuskina *et al.*, 2014), would be the sum of two theoretical end-members: 75% $Ca_4(Fe^{3+}{}_{12})O_4[Fe^{3+}{}_{12}]O_{36}$ + 25% $Ca_4(Mg_{12})O_4[Si_{12}]O_{36}$.

However, the problem of defining proper end-member formulae for this group should be addressed by taking into account structural and crystal-chemical data. For the dorrite–khesinite series in particular, we can ground on structural data for holotype khesinite together with crystal-chemical data on khesinite from other localities (Fig. 5, Tables 1 and 6). One octahedral site and one tetrahedral site differ sharply in size from other sites (Table 4): *M*5 is the largest octahedral site with average distance *M*–O = 2.19 Å compared to *M*–O = 2.04–2.07 Å for the other sites. Similarly, *T*4 is the smallest tetrahedral site with *T*–O = 1.65 Å, compared to *T*–O = 1.75–1.87 Å for the other sites. The *T*4 site is 94% occupied by Si (Table 3) in holotype khesinite, and Si averages 2.2(2) apfu for all khesinite analyses (~70) from paralava, as shown in the Fe^{3+}–Al–Si diagram (Fig. 5). To achieve charge balance for incorporation of Si at *T*4, divalent cations occupy an octahedral site, in our case Mg(+Ca) at *M*5. Considering the strong differentiation of the *M*5 site, we suggest using $Ca_4M'_2M_{10}O_4[T_{12}O_{36}]$ or the simplified formula $Ca_4M'_2M_{10}T_{12}O_{40}$ as end-member formula for minerals of the dorrite–khesinite series, where the species-defining *M*′ corresponds to the large octahedral site. Consequently, the empirical crystal-chemical formula of khesinite $Ca_4(Fe^{3+}{}_{8.528}Mg_{1.635}Ca_{0.898}Ti^{4+}{}_{0.336}Ni^{2+}{}_{0.217}Mn^{2+}{}_{0.155}Cr^{3+}{}_{0.132}Fe^{2+}{}_{0.098})_{\Sigma 12}O_4[(Fe^{3+}{}_{6.827}Al_{2.506}Si_{2.667})_{\Sigma 12}O_{36}]$ can be written with separated *M*5 sites: $Ca_4(Mg_{1.102}Ca_{0.898})_{\Sigma 2}(Fe^{3+}{}_{8.528}Mg_{0.533}Ti^{4+}{}_{0.336}Ni^{2+}{}_{0.217}Mn^{2+}{}_{0.155}Cr^{3+}{}_{0.132}Fe^{2+}{}_{0.098})_{\Sigma 10}O_4[(Fe^{3+}{}_{6.827}Al_{2.506}Si_{2.667})_{\Sigma 12}O_{36}]$, simplified to $Ca_4Mg_2Fe^{3+}{}_{10}O_4[(Si_2Fe^{3+}{}_{10})O_{36}]$. The corresponding end-member formula for dorrite is $Ca_4Mg_2Fe^{3+}{}_{10}O_4[(Si_2Al_{10})O_{36}]$. These two formulae meet the criteria for an end-member, as valency-imposed double occupation occurs at only one site (Hawthorne, 2002), the undifferentiated *T* site. Some analyses of khesinite (Table 1, analyses 2, 3) show for *M*′ Ca contents >1 apfu and Mg < 1 apfu, which suggests a potential new mineral species with composition $Ca_4Ca_2Fe^{3+}{}_{10}O_4[(Si_2Fe^{3+}{}_{10})O_{36}]$.

The empirical formula of addibischoffite (Ma *et al.*, 2016), $(Ca_{2.00})(Al_{2.55}Mg_{1.73}V^{3+}{}_{1.08}Ti^{3+}{}_{0.50}Ca_{0.09}Fe^{2+}{}_{0.05})_{\sum 6.01}(Al_{4.14}Si_{1.86})O_{20}$, can be simplified to (on a 40 O basis) $Ca_4Mg_2(Mg_2Al_8)O_4[(Si_4Al_8)O_{36}]$, which, differentiating only one *M* site and applying the dominant-valence rule, leads to the same type of end-member formula as proposed for the khesinite–dorrite series: $Ca_4Mg_2Al_{10}O_4[(Si_2Al^{3+}{}_{10})O_{36}]$, making addibischoffite the Al-analogue of khesinite in terms of both the *M* and *T* sites, whereas dorrite is an Al analogue in terms of only the *T* sites.

8. Genetic aspects of khesinite formation

The ferrites (all iron as Fe^{3+}): magnesioferrite $MgFe_2O_4$, trevorite $NiFe_2O_4$, cuprospinel $CuFe_2O_4$, delafossite $CuFeO_2$, harmunite $CaFe_2O_4$; brownmillerite $Ca_2Fe(Al,Fe)O_5$ and srebrodolskite $Ca_2Fe(Fe,Al)O_5$; shulamitite $Ca_3TiFe(Al,Fe)O_8$ and its analogue $Ca_3TiFe(Fe,Al)O_8$; barioferrite $BaFe_{12}O_{19}$, "calcioferrite" $CaFe_{12}O_{19}$, khesinite $Ca_4Mg_2Fe_{10}O_4[Si_2Fe_{10}O_{36}]$, dorrite $Ca_4Mg_2Fe_{10}O_4[Si_2Al_{10}O_{36}]$, and the CFF phases $Ca_2Mg_2Fe_{10}(Al,Fe)_4O_{25}$ and $Ca_2Mg_2Fe_{10}(Fe,Al)_4O_{25}$ have been found in pyrometamorphic rocks of the Hatrurim Complex (Murashko *et al.*, 2010; Sharygin *et al.*, 2013; Galuskina *et al.*, 2014 and this study). Primary magnesiochromite $Mg(Cr,Fe)_2O_4$, "hexaferrite" with composition $Ca(Cr,Fe)_{12}O_{19}$ and the Cr-analogue of khesinite $Ca_4Mg_2Cr_{10}O_4[(Si_2Fe_{10})O_{36}]$ were found in gehlenite hornfels. Hematite (Fe_2O_3) is widely distributed in different types of rocks of the Hatrurim Complex. Magnetite (Fe^{2+} > Mg), usually with high Ni, Cu and Zn contents, is rarely noted in paralavas.

Three main phases, SFCA and SFCA-I (Si-bearing systems) and CFF (low-Si systems), are key intermediate phases in the sintering process of iron ores (*e.g.* Scarlett *et al.*, 2004; Webster *et al.*, 2014; Ding *et al.*, 2015). The phase SFCA, $Ca_4Fe^{3+}{}_{12}(Fe^{3+},Al)_{12}O_{40}$, is a structural analogue of minerals of the dorrite–khesinite series, *i.e.* polysome ⟨PS⟩, whereas SFCA-I, $Ca_6Fe^{2+}{}_2(Fe^{3+},Al)_{32}O_{56}$, polysome ⟨PSS⟩, has no natural analogue (Mumme, 2003; Grew *et al.*, 2008). The formula for SFCA-1 normalized to 7O is $Ca_{0.75}Fe^{2+}{}_{0.25}(Fe^{3+},Al)_4O_7 \approx CaFe_4O_7$, *i.e.* the formula of "grandiferrite" described from burnt coal dumps in Chelyabinsk and porcellanite in the Czech Republic (Chesnokov *et al.*, 1998; Záček *et al.*,

Table 8. Composition of ferrites from flamite–gehlenite hornfels.

Sample	IS74A					IS104		JB1
Mineral	Sp	Shl	Srbr	Dor	CFF	Sp	CFF	CFF
Fig. 4	1			2	3	4	5	
wt.%	1	2	3	4	5	6	7	8
ZrO_2	n.d.	0.54	n.d.	n.d.	n.d.	n.d.	n.d.	n.d.
TiO_2	0.05	20.29	0.54	0.57	0.10	n.d.	0.35	0.13
SiO_2	n.d.	0.79	0.34	4.99	n.d.	n.d.	0.10	1.4
Fe_2O_3	44.99	25.57	44.86	51.44	65.51	43.11	63.74	73.15
Cr_2O_3	0.91	0.09	0.41	0.51	0.73	3.64	1.46	0.43
Al_2O_3	29.17	7.49	9.31	25.61	16.99	27.49	16.16	7.12
CuO	n.d.	n.d.	n.d.	n.d.	0.21	0.26	n.d.	0.56
ZnO	1.95	n.d.	n.d.	n.d.	0.74	0.8	n.d.	n.d.
NiO	0.43	n.d.	n.d.	n.d.	0.38	0.93	0.30	0.62
FeO		0.52	0.53			0.12		
MnO	0.24	n.d.	0.15	n.d.	0.22	n.d.	n.d.	0.23
CaO	0.43	42.9	43.4	13.25	7.18	0.596	9.14	9.22
MgO	21.89	0.22	0.15	3.28	7.68	21.19	7.51	6.45
Total	100.08	98.42	99.7	99.64	99.73	98.13	98.76	99.31
Calc. on	4 O	8 O	5 O	40 O	25 O	4 O	25 O	25 O
Ca		3.024	1.998	4.000	1.534		1.971	2.071
Mg					2.284		2.029	1.929
Ni					0.060			
Cu					0.032			
Zn					0.109			
Mn^{2+}			0.005		0.037			
X		*3.024*	*2.003*	*4*	*4.056*		*4*	*4*
Ca	0.013			0.242		0.019		
Mg	0.942	0.021	0.010	1.462		0.933	0.224	0.088
Ni	0.010					0.022	0.049	0.104
Cu						0.006		0.088
Zn	0.042					0.017		
Mn^{2+}	0.006							0.042
Fe^{2+}		0.029	0.019			0.003		
Al	0.969					0.915		
Cr^{3+}	0.021	0.005	0.014	0.120	0.115	0.085	0.232	0.072
Fe^{3+}		0.899	0.936	10.078	9.827		9.509	9.589
Ti^{4+}	0.001	1.004	0.018	0.127	0.015		0.053	0.020
Zr		0.017						
M	*2.004*	*1.975*	*0.997*	*12.029*	*9.957*	*2*	*10.067*	*10.003*
Al	0.023	0.581	0.471	9.019	3.993	0.042	3.834	1.758
Fe^{3+}	0.977	0.367	0.514	1.490	0.007	0.958	0.146	1.950
Si		0.052	0.015	1.491			0.020	0.292
T	*1*	*1*	*1*	*12*	*4*	*1*	*4*	*4*

Note: Fe^{2+}/Fe^{3+} ratio calculated from stoichiometry. Abbreviations: Sp – spinel, Shl – shulamitite, Srbr – srebrodolskite, Drr – dorrite, CFF – synthetic calcium ferrite phase.

2015). In our opinion the phase CFF, $Ca_3Fe^{2+}Fe^{3+}{}_{14}O_{25}$, has a natural analogue in rocks of the Hatrurim Complex (Table 8, analyses 5, 7, 8). Normalization to 7O gives $Ca_{0.84}Fe^{2+}{}_{0.28}Fe^{3+}{}_{3.92}O_7 \approx CaFe_4O_7$, which is also close to "grandiferrite". However, distinguishing natural analogues of CFF and SFCA-I with a high content of Mg, which may substitute for both Ca and Fe^{3+}, requires structural investigation (Table 9).

Temperature and composition of initial furnace feed are the main parameters defining the formation of synthetic SFCA phases. In processes of iron-ore agglomeration, ferrite crystallization begins with the C_2F phase – srebrodolskite $Ca_2Fe_2O_5$ (Ca/Fe ≈ 1; 750–780 °C), which at higher temperature (>950 °C) reacts with Fe_2O_3 to form the CF phase – harmunite $CaFe_2O_4$, (Ca/Fe ≈ 0.5) (Scarlett *et al.*, 2004). Harmunite is a new mineral found in pyrometamorphic rocks of the Hatrurim Complex. It is assumed that its formation temperature is significantly below 1000 °C as a result of crystallization from sulphate–chloride-bearing melts (Galuskina *et al.*, 2014). In sintering processes, the SFCA and SFCA-I phases (Ca/Fe ≈ 0.2) begin to form from pre-existing

Table 9. Crystal chemical and end-member formulae of the khesinite–dorrite series.

Polyhedral site	Octahedral site		Tetrahedral site		
Old formulae, do not conform to the rules of IMA CNMNC					
$^{VII}(A1_2A2_2)_{\Sigma4}$	$^{VI}(M1M2M3_2M4_2M5_2M6_2M7_2)_{\Sigma12}$		O_4	$(T1_2T2_2T3_2T4_2T5_2T6_2)_{\Sigma12}O_{36}$	Structural formula of series
Ca_4	$(Mg_3Fe^{3+}{}_9)$		O_4	$[Si_3Al_8Fe^{3+}O_{36}]$	Originally proposed formula of dorrite (Grew *et al.*, 2008)
Ca_4	$(Fe^{3+}{}_9Mg_3)$		O_4	$[Fe^{3+}{}_9Si_3O_{36}]$	Originally proposed formula of khesinite (Galuskina *et al.*, 2015)
Ca_4	$(Fe^{3+}{}_{8.528}Mg_{1.635}Ca_{0.898}Ti^{4+}{}_{0.336}Ni^{2+}{}_{0.217}Mn^{2+}{}_{0.155}Cr^{3+}{}_{0.132}Fe^{2+}{}_{0.098})_{\Sigma12}$		O_4	$[(Fe^{3+}{}_{6.827}Al_{2.506}Si_{2.667})_{\Sigma12}O_{36}]$	Empirical formula of khesinite, this study
New proposition based on the rules of IMA CNMNC (Hawthorne, 2002; Hatert & Burke, 2008)					
$^{VII}(A1_2A2_2)_{\Sigma4}$	$M5_2$	$^{VI}(M1M2M3_2M4_2M6_2M7_2)_{\Sigma10}$	O_4	$[(T1_2T2_2T3_2T4_2T5_2T6_2)_{\Sigma12}O_{36}]$	Structural formula of series
Ca_4	M'_2	M_{10}	O_4	$[T_{10}Si_2O_{36}]$	Simplified structural formula of series
Ca_4	$(Mg_{1.102}Ca_{0.898})_{\Sigma2}$	$(Fe^{3+}{}_{8.528}Mg_{0.533}Ti^{4+}{}_{0.336}Ni^{2+}{}_{0.217}Mn^{2+}{}_{0.155}Cr^{3+}{}_{0.132}Fe^{2+}{}_{0.098})_{\Sigma10}$	O_4	$[(Fe^{3+}{}_{6.827}Al_{2.506}Si_{2.667})_{\Sigma12}O_{36}]$	Empirical formula of khesinite
Ca_4	Mg_2	$Fe^{3+}{}_{10}$	O_4	$[Si_2Fe^{3+}{}_{10}O_{36}]$	New proposed end-member formula of khesinite
Ca_4	Mg_2	$Fe^{3+}{}_{10}$	O_4	$[Si_2Al_{10}O_{36}]$	New proposed end-member formula of dorrite
Ca_4	Ca_2	$Fe^{3+}{}_{10}$	O_4	$[Si_2Fe^{3+}{}_{10}O_{36}]$	New proposed end-member formula of a potentially new mineral of the series
Ca_4	Ca_2	$Cr^{3+}{}_{10}$	O_4	$[Si_2Fe^{3+}{}_{10}O_{36}]$	Our data

ferrites above 1050 °C as a result of solid-state reactions in the $CaO–Fe_2O_3$ system; Al_2O_3 impurities extend their stability fields to lower temperatures (Scarlett *et al.*, 2004; Webster *et al.*, 2012; Gan *et al.*, 2015). High bulk SiO_2 contents reduce the stability range of the phases SFCA-I and CFF, which contain little or no Si (Webster *et al.*, 2014; Ding *et al.*, 2015; Gan *et al.*, 2015). Formation of SFCA-type phases increases above 1200 °C, when melting of srebrodolskite and harmunite begins (Scarlett *et al.*, 2004).

Holotype khesinite crystallized in paralava from melt, sometimes forming crystals, but more often reaction rims on magnesioferrite (Fig. 6). Khesinite occurs with pseudowollastonite and flamite. Formation of pseudowollastonite and flamite takes place at or above 1200 °C in paralavas of the Hatrurim Complex (Seryotkin *et al.*, 2012; Sokol *et al.*, 2015). Absence of srebrodolskite and harmunite in these paralava rocks is also evidence of high-temperature formation of khesinite (~1200–1250 °C). Paralava with khesinite fills the interstices between large gehlenite, rankinite, schorlomite and pseudowollastonite crystals. Here khesinite is a product of crystallization of isolated portions of residual melt.

In gehlenite–flamite hornfels, genesis of minerals of the khesinite–dorrite series is related to high-temperature alterations of early formed gehlenite–flamite hornfels affected by sulphate- and halogen-bearing melts/fluids generated during pyrometamorphism. These high-temperature fluids penetrated the rock through channels, thin cracks and intergranular boundaries and reacted with early-formed minerals. The formation sequence of ferrites in gehlenite–flamite pyrometamorphic rocks can be presented as follows (see Fig. 6b and d–f): (1) during prograde metamorphism hematite formed after pyrite from sedimentary rocks, which was replaced by Ca-bearing magnesioferrite at rising temperature; (2) there was possibly a period during which the system cooled, resulting in crystallization of platy "hexaferrite" $CaFe_{12}O_{19}$ in the magnesioferrite matrix accompanied by formation of a silicocarnotite–rankinite symplectite; (3) local heat injection by fluid/melt into the pyrometamorphic rocks resulted in partial dissolution of magnesioferrite and overgrowth by khesinite. The Ca-"hexaferrite" was replaced by barioferrite, whereas barite crystallized in vesicles in altered magnesioferrite (Fig. 6e).

Therefore, crystallization of khesinite, both in paralavas and hornfels, resulted from injection of melts/fluids, which reacted with earlier phases, *i.e.* khesinite is a product of high-temperature alteration of pre-existing pyrometamorphic rocks. Melts/fluids were mainly generated during formation of pyrometamorphic hornfels, probably at peak temperatures. Melts penetrated the hornfels along microcracks and channels or filled larger cracks forming paralava bodies. A similar mechanism of high-temperature alteration of primary pyrometamorphic rocks with participation of liquid phase (melt, fluid) was proposed

by us (Galuskin *et al.*, 2016) for the formation of big ternesite metacrystals within fine-grained larnite–ye'elimite–brownmillerite–fluorellestadite rocks (clinker association).

Thus, we assume that during pyrometamorphism, melts (fluids) were produced at local hot spots. These migrating fluids altered earlier formed rocks containing typical clinker assemblages.

Acknowledgements: The authors thank two reviewers (anonymous reviewer#1 and Ulf Hålenius) for their careful reviews that improved the early version of the manuscript. The work was supported by the National Science Centre (NCN) of Poland, grant no. UMO-2013/11/B/ST10/00272.

References

Bentor, Y. (1960): Israel. *in* "Lexique stratigraphique international, part 10.2, Asie", Centre National de la Recherche Scientifique, Paris, Vol. **III**, 80 p.

Bonaccorsi, E., Merlino, S., Pasero, M. (1990): Rhönite: structural and microstructural features, crystal chemistry and polysomatic relationships. *Eur. J. Mineral.*, **2**, 203–218.

Bruker (2012): SMART and SAINT-Plus. Versions 6.01. Bruker AXS Inc., Madison, Wisconsin, USA.

Cannillo, E., Mazzi, F., Fang, J.H., Robinson, P.D., Ohya, Y. (1971): The crystal structure of aenigmatite. *Am. Mineral.*, **56**, 427–446.

Chesnokov, B.V., Vilisov, V.A, Bazhenova, L.F., Bushmakin, A.F., Kotlyarov, V.A. (1993): New minerals from the burned dumps of the Chelyabinsk coal basin (fifth communication). *Ural Mineral. Collect.*, **2**, 3–8.

Chesnokov, B., Kotrly, M., Nisanbajev, T. (1998): Brennende Abraumhalden und Aufschlüsse im Tscheljabinsker Kohlenbecken - eine reiche Mineralienküche. *Mineralien-Welt*, **9**, 54–63.

Chesnokov, V.B., Scherbakova, E.P., Nishanbaev, T.P. (2008): Minerals of burned dumps of the Chelyabinsk Coal Basin. Institute of Mineralogy, RAS Ural Branch, Miass, 139 p.

Cosca, M.A., Rouse, R.R., Essene, E.J. (1988): Dorrite [$Ca_2(Mg_2Fe^{3+}_4)(Al_4Si_2)O_{20}$], a new member of the aenigmatite group from a pyrometamorphic melt-rock. *Am. Mineral.*, **73**, 1440–1448.

Ding, X., Guo, X.-M., Ma, C-Y., Tang, K., Zhao, Y-D. (2015): Effect of SiO_2 on the crystal structure stability of SFC at 1473 K (1200 °C). *Metall. Mater. Trans. B*, **46**, 1146–1153.

Foit, F.F., Jr., Hooper, R.L., Rosenberg, P.E. (1987): An unusual pyroxene, melilite, and iron oxide mineral assemblage in a coal-fire buchite from Buffalo, Wyoming. *Am. Mineral.*, **72**, 137–147.

Gan, M., Fan, X., Chen, X. (2015): Calcium ferrite generation during iron ore sintering – crystallization behavior and influencing factors, chapter 12, 301–321. *in* "Advanced topics in crystallization", Y. Mastai, ed. InTech, 370 p.

Galuskin, E.V., Gfeller, F., Galuskina, I.O., Pakhomova, A., Armbruster, T., Vapnik, Y., Włodyka, R., Dzierżanowski, P., Murashko, M. (2015): New minerals with a modular structure derived from hatrurite from the pyrometamorphic Hatrurim Complex. Part II. Zadovite, $BaCa_6[(SiO_4)(PO_4)](PO_4)_2F$ and aradite, $BaCa_6[(SiO_4)(VO_4)](VO_4)_2F$, from paralavas of the Hatrurim Basin, Negev Desert, Israel. *Mineral. Mag.*, **79**, 1073–1087.

Galuskin, E.V., Galuskina, I.O., Gfeller, F., *et al.* (2016): Silicocarnotite, $Ca_5[(SiO_4)(PO_4)](PO_4)$, a new "old" mineral from the Negev Desert, Israel, and the ternesite–silicocarnotite solid solution: indicators of high-temperature alteration of pyrometamorphic rocks of the Hatrurim Complex, Southern Levant. *Eur. J. Mineral.*, **1**, 105–123.

Galuskina, I.O., Vapnik, Y., Prusik, K., Dzierżanowski, P., Murashko, M., Galuskin, E.V. (2013): Gurimite, IMA 2013-032. CNMNC newsletter no. 16, August 2013, page 2708. *Mineral. Mag.*, **77**, 2695–2709.

Galuskina, I.O., Vapnik, Ye., Lazic, B., Armbruster, T., Murashko, M., Galuskin, E.V. (2014): Harmunite $CaFe_2O_4$: a new mineral from the Jabel Harmun, West Bank, Palestinian Autonomy, Israel. *Am. Mineral.*, **99**, 965–975.

Galuskina, I.O., Galuskin, E.V., Prusik, K., Vapnik, Y., Dzierżanowski, P., Murashko, M. (2015): Hexacelsian, IMA2015-045. CNMNC newsletter no. 27, October 2015, page 1224. *Mineral. Mag.*, **79**, 1229–1236.

Gasparik, T., Parise, J.B., Reeder, R.J., Young, V.G., Wilford, W.S. (1999): Composition, stability and structure of a new member of the aenigmatite group, $Na_2Mg_{4+x}Fe^{3+}_{2-2x}Si_{6+x}O_{20}$, synthesized at 13–14 GPa. *Am. Mineral.*, **84**, 257–266.

Gatel, P., Záček, V., Kruszewski, Ł., Devouard, B., Thiéry, V., Eytier, C., Eytier, J.-R., Favreau, G., Vigier, J., Stracher, G.B. (2015): Combustion mineralogy and petrology of oil-shale slags in Lapanouse, Sévérac-le-Château, Aveyron, France: analogies with hydrocarbon fires. *in* "Coal and peat fires: a global perspective, volume 3: case studies – coal fires", G.B. Stracher, A. Prakash and E.V. Sokol, eds., Vol. 28. Elsevier, 681–742.

Gfeller, F., Widmer, R., Krüger, B., Galuskin, E.V., Galuskina, I.O., Armbruster, T. (2015): The crystal structure of flamite and its relation to Ca_2SiO_4 polymorphs and nagelschmidtite. *Eur. J. Mineral.*, **27**, 755–769.

Grew, E.S., Hålenius, U., Pasero, M., Barbier, J. (2008): Recommended nomenclature for the sapphirine and surinamite groups (sapphirine supergroup). *Mineral. Mag.*, **72**, 839–876.

Gross, S. (1977): The mineralogy of the Hatrurim Formation, Israel. *Geol. Surv. Israel B.*, **70**, 1–80.

Hamilton, J.D.G., Hoskins, B.F., Mumrne, W.G., Borbridge, W.E., Montague, M.A. (1989): The crystal structure and crystal chemistry of $Ca_{2.3}Mg_{0.8}Al_{1.5}Si_{1.1}Fe_{8.3}O_{20}$ (SFCA): solid solution limits and selected phase relationships of SFCA in the SiO_2–Fe_2O_3–CaO (–Al_2O_3) system. *N. Jb. Mineral. Abh.*, **16l**, l–26.

Hatert, F. & Burke, E.A.J. (2008): The IMA-CNMNC dominant-constituent rule revisited and extended. *Can. Mineral.*, **46**, 717–728.

Hawthorne, F. (2002): The use of end-member charge-arrangements in defining new mineral species and heterovalent substitutions in complex minerals. *Can. Mineral.*, **40**, 699–710.

Hwang, S.-L., Shen, P., Chu, H.-T., Yui, T.-F., Varela, M.-E., Iizuka, Y. (2014): Kuratite, IMA 2013-109. CNMNC newsletter no. 19, February 2014, page 168. *Mineral. Mag.*, **78**, 165–170.

Kolev, N., Iliev, M.N., Popov, V.N., Gospodinov, M. (2003): Temperature-dependent polarized Raman spectra of $CaFe_2O_4$. *Solid State Commun.*, **128**, 153–155.

Liles, D.C., de Villiers, J.P.R., Kahlenberg, V. (2016): Refinement of iron ore sinter phases: a silico-ferrite of calcium and aluminium (SFCA) and an Al-free SFC, and the effect on phase quantification by X-ray diffraction. *Mineral. Petrol.*, **110**, 141–147.

Ma, C. & Krot, A.N. (2015): Addibischoffite, IMA 2015-001. CNMNC newsletter no. 25, June 2015, page 532. *Mineral. Mag.*, **79**, 529–535.

Ma, C., Krot, A.N., Nagashima, K., Tschauner, O. (2014): Warkite, IMA 2013-129. CNMNC newsletter no. 20, June 2014, page 552. *Mineral. Mag.*, **78**, 549–558.

Ma, C., Paque, J., Tschauner, O. (2015): Beckettite, IMA 2015-001. CNMNC newsletter no. 25, June 2015, page 531. *Mineral. Mag.*, **79**, 529–535.

Ma, C., Krot, A.N., Nagashima, K. (2016): Discovery of new mineral addibischoffite, $Ca_2Al_6Al_6O_{20}$, in a Ca–Al-rich refractory inclusion from the Acfer 214 CH3 meteorite. Abstr. In "79th Annual Meeting of the Meteoritical Society", Berlin, Germany, 7–12 August 2016, no. 6016.

Merlino, S. & Pasero, M. (1997): Polysomatic approach in the crystal chemical study of minerals. Chapter 4. *in* "Modular aspects of minerals", S. Merlino, ed. Eötvös University Press, Budapest, Vol. **1**, 297–312. EMU Notes in Mineralogy.

Mills, S.J., Hatert, F., Nickel, E.H., Ferraris, G. (2009): The standardisation of mineral group hierarchies: application to recent nomenclature proposals. *Eur. J. Mineral.*, **21**, 1073–1080.

Mumme, W.G. (1988): A note on the relationship of $Ca_{2.3}Mg_{0.8}Al_{1.5}Si_{1.1}Fe_{8.3}O_{20}$ (SFCA) with aenigmatite group minerals and sapphirine. *N. Jb. Mineral. Mh.*, **1988** (8), 359–366.

— (2003): The crystal structure of SFCA-II, $Ca_{5.1}Al_{9.3}Fe^{3+}_{18.7}Fe^{2+}_{0.9}O_{48}$ a new homologue of the aenigmatite structure-type, and structure refinement of SFCA-type, $Ca_2Al_5Fe_7O_{20}$. Implication for the nature of the "ternary-phase solid-solution" previously reported in the $CaO–Al_2O_3$–iron oxide system. *N. Jb. Mineral. Abh.*, **178**, 307–335.

Mumme, W.G., Clout, J.M.F., Gable, R.W. (1998): The crystal structure of SFCA-I, $Ca_{3.18}Fe^{3+}_{14.66}Al_{1.34}Fe^{2+}_{0.82}O_{28}$, a homologue of the aenigmatite structure type, and new crystal structure refinements of β-CFF, $Ca_{2.99}Fe^{3+}_{14.30}Fe^{2+}_{0.55}O_{25}$ and Mg-free SFCA, $Ca_{2.45}Fe^{3+}_{9.04}Al_{1.74}Fe^{2+}_{0.16}Si_{0.6}O_{20}$. *N. Jb. Mineral. Abh.*, **173**, 93–117.

Murashko, M.N., Chukanov, N.V., Mukhanova, A.A., et al. (2010): Barioferrite $BaFe^{3+}_{12}O_{19}$ – a new magnetoplumbite-group mineral from Hatrurim Formation, Israel. *P. Russ. Miner. Soc.*, **139**, 22–31 [in Russian].

Novikov, I., Vapnik, Ye., Safonova, I. (2013): Mud volcano origin of the Mottled Zone, South Levant. *Geosci. Front.*, **4**, 597–619.

Seryotkin, Yu.V., Sokol, E.V., Kokh, S.N. (2012): Natural pseudowollastonite: crystal structure, associated minerals, and geological context. *Lithos*, **134–135**, 75–90.

Scarlett, N.V.Y., Pownceby, M.I., Madsen, I.C., Christensen, A.N. (2004): Reaction sequences in the formation of silico-ferrites of calcium and aluminum in iron ore sinter. *Metall. Mater. Trans. B: Process Metall. Mater. Process. Sci.*, **35**, 929–936.

Sharygin, V.V., Lazic, B., Armbruster, T.M., Murashko, M.N., Wirth, R., Galuskina, I.O., Galuskin, E.V., Vapnik, Y., Britvin, S.N., Logvinova, A.M. (2013): Shulamitite $Ca_3TiFe^{3+}AlO_8$ – a new perovskite-related mineral from Hatrurim Basin. *Eur. J. Mineral.*, **25**, 97–111.

Sheldrick, G.M. (1996): SADABS. University of Göttingen, Germany.

— (2008): A short history of SHELX. *Acta Crystallogr. A*, **64**, 112–122.

Sokol, E.V., Gaskova, O.L., Kokh, S.N., Kozmenko, O.A., Seryotkin, Y.V., Vapnik, Y., Murashko, M. (2011): Chromatite and its Cr^{3+}- and Cr^{6+}-bearing precursor minerals from the Nabi Musa Mottled Zone complex, Judean Desert. *Am. Mineral.*, **96**, 659–674.

Sokol, E.V., Seryotkin, Y.V., Kokh, S.N., Vapnik, Y., Nigmatulina, E.N., Goryainov, S.V., Belogub, E.V., Sharygin, V.V. (2015): Flamite $(Ca, Na, K)_2(Si, P)O_4$, a new mineral from the ultrahigh-temperature combustion metamorphic rocks, Hatrurim Basin, Negev Desert, Israel. *Mineral. Mag.*, **79**, 583–596.

Sugiyama, K., Monkawa, A., Sugiyama, T. (2005): Crystal structure of the SFCAM phase, $Ca_2(Ca, Fe, Mg, Al)_6(Fe, Al, Si)_6O_{20}$. *ISIJ Int.*, **45**, 560–568.

Vapnik, Y., Sharygin, V.V., Sokol, E.V., Shagam, R. (2007): Paralavas in a combustion metamorphic complex: Hatrurim Basin, Israel. *Rev. Eng. Geol.*, **18**, 1–21.

Webster, N.A.S., Pownceby, M.I., Madsen, I.C., Kimpton, J.A. (2012): Silico-ferrite of calcium and aluminum (SFCA) iron ore sinter bonding phases: new insights into their formation during heating and cooling. *Metall. Mater. Trans.*, **43B**, 1344–1357.

Webster, N.A.S., Pownceby, M.I., Madsen, I.C., Studer, A.J., Manuel, J.R., Kimpton, J.A. (2014): Fundamentals of silico-ferrite of calcium and aluminum (SFCA) and SFCA-I iron ore sinter bonding phase formation: effects of $CaO:SiO_2$ ratio. *Metall. Mater. Trans. B*, **45**, 2097–2105.

Zvyagin, B.B. (1997): Modular analysis of crystal structures. Chapter 5. in "Modular aspects of minerals", S. Merlino, ed. *Eötvös University Press, Budapest*, **1**, 345–372. EMU Notes in Mineralogy.

Záček, V., Skála, R., Dvorák, Z. (2015): Combustion metamorphism in the Most Basin. *in* "Coal and Peat Fires: A Global Perspective, volume 3: case studies – coal fires", G.B. Stracher, A. Prakash,E.V. Sokol, eds., 6. Elsevier, 162–202.

Received 26 May 2016
Modified version received 2 July 2016
Accepted 5 September 2016